Three-dimensional visualization of fossil flowers, fruits, seeds, and other plant remains using synchrotron radiation X-ray tomographic microscopy (SRXTM): new insights into Cretaceous plant diversity

Authors: Friis, Else Marie, Marone, Federica, Pedersen, Kaj Raunsgaard, Crane, Peter R., and Stampanoni, Marco

Source: Journal of Paleontology, 88(4) : 684-701

Published By: The Paleontological Society

URL: https://doi.org/10.1666/13-099

Journal of Paleontology, 88(4), 2014, p. 684–701

0022-3360/14/0088-684$03.00
DOI: 10.1666/13-099

THREE-DIMENSIONAL VISUALIZATION OF FOSSIL FLOWERS, FRUITS, SEEDS, AND OTHER PLANT REMAINS USING SYNCHROTRON RADIATION X-RAY TOMOGRAPHIC MICROSCOPY (SRXTM): NEW INSIGHTS INTO CRETACEOUS PLANT DIVERSITY

ELSE MARIE FRIIS,[1] FEDERICA MARONE,[2] KAJ RAUNSGAARD PEDERSEN,[3] PETER R. CRANE,[4] AND MARCO STAMPANONI[2,5]

[1]Department of Palaeobiology, Swedish Museum of Natural History, SE-104 05 Stockholm, Sweden, <else.marie.friis@nrm.se>;
[2]Swiss Light Source, Paul Scherrer Institute, CH-5232 Villigen PSI, Switzerland, <federica.marone@psi.ch>; <marco.stampanoni@psi.ch>;
[3]Department of Geology, University of Aarhus, DK-8000 Aarhus, Denmark, <krp@geo.au.dk>; [4]Yale School of Forestry and Environmental Studies 195 Prospect Street, New Haven, CT 06511, USA, <peter.crane@yale.edu>; and [5]Institute for Biomedical Engineering, ETZ F 85, Swiss Federal Institute of Technology Zürich, Gloriastrasse 35, 8092 Zürich, <stampanoni@biomed.ee.ethz.ch>

ABSTRACT—The application of synchrotron radiation X-ray tomographic microscopy (SRXTM) to the study of mesofossils of Cretaceous age has created new possibilities for the three-dimensional visualization and analysis of the external and internal structure of critical plant fossil material. SRXTM provides cellular and subcellular resolution of comparable or higher quality to that obtained from permineralized material using thin sections or the peel technique. SRXTM also has the advantage of being non-destructive and results in the rapid acquisition of large quantities of data in digital form. SRXTM thus refocuses the effort of the investigator from physical preparation to the digital post-processing of X-ray tomographic data, which allows great flexibility in the reconstruction, visualization, and analysis of the internal and external structure of fossil material in multiple planes and in two or three dimensions. A review of recent applications in paleobotany demonstrates that SRXTM will dramatically expand the level of information available for diverse fossil plants. Future refinement of SRXTM approaches that further increases resolution and eases digital post-processing, will transform the study of mesofossils and create new possibilities for advancing paleobotanical knowledge. We illustrate these points using a variety of Cretaceous mesofossils, highlighting in particular those cases where SRXTM has been essential for resolving critical structural details that have enhanced systematic understanding and improved phylogenetic interpretations.

INTRODUCTION

THE PAST thirty to forty years have seen significant advances in understanding patterns of structural diversification during the early phases of angiosperm evolution. Central in these developments has been the discovery in Cretaceous sediments of small 3-D vegetative and reproductive structures (mesofossils), including angiosperm flowers, fruits, and seeds (Tiffney, 1977; Friis and Skarby, 1981; see also references in Friis et al., 2011). These fossils, which are preserved both as lignitized specimens and as charcoal, often have exquisite preservation of complex form as well as superb preservation of cellular and other internal details. Initially, this material was studied with considerable success using scanning electron microscopy (SEM), occasionally supplemented by conventional serial sectioning after embedding the specimens in plastic. Over time technical advances in SEM also improved resolution in the routine microscopy of surface features.

More recently, the application of synchrotron radiation X-ray tomographic microscopy (SRXTM) has provided a new way of studying diverse mesofossils through the digital capture of high-resolution, large, X-ray tomographic, datasets. Unlike with conventional sectioning, these datasets are created without damage to the specimen, and they enable the reconstruction, visualization, and analysis of the internal and external structure of critical fossil material with new flexibility. Two-dimensional sections can be constructed in multiple orientations, 3-D reconstructions can be created and manipulated, and complex specimens, such as flowers, can be dissected digitally rather than physically. SRXTM greatly enhances the information that can be obtained from fossil plants for comparative and phylogenetic studies (Friis et al., 2007).

Extensive datasets on fossil plants have been accumulated from SRXTM analyses at the Tomcat beamline (Stampanoni et al., 2006) at the Swiss Light Source (SLS) covering material from the Carboniferous (Scott et al., 2009), Permian (Slater et al., 2011), Cretaceous (Friis et al., 2007; von Balthazar et al., 2007; von Balthazar et al., 2008; Friis et al., 2009b; Friis et al., 2010; Friis and Pedersen, 2011; Heřmanová et al., 2011; von Balthazar et al., 2011; Friis and Pedersen, 2012; Friis et al., 2013a; Friis et al., 2013b; Friis et al., 2014a, 2014b; Mendes et al., 2014), and Cenozoic (Smith et al., 2009a; Smith et al., 2009b; Collinson et al., 2013a; Collinson et al., 2013b). The only other published studies on Cretaceous flowers examined at other beamlines is that of *Glandulocalyx upatoiensis* Schönenberger et al., 2012, analyzed mainly at the beamline 2-BM of the Advanced Photon Source at the U.S. Department of Energy Argonne National Laboratory, but also at the BL20B2 beamline of the Super Proton ring-8 GeV (SPring-8) at the Japan Synchrotron Radiation Research Institute (Schönenberger et al., 2012), and unnamed flower studied at the beamlines BM05, ID19, and ID22 at ESRF, Grenoble (Moreau et al., 2014). There are also now several studies of extant floral structures using laboratory based X-ray CT (e.g., Staedler et al., 2013).

In this paper we provide an overview of the SRXTM techniques applied so far to understand and visualize the detailed structure of Cretaceous fossil flowers and other plant mesofossils. We focus on examples from the very substantial datasets collected at the SLS and highlight those cases where SRXTM has resolved critical structural details that have

improved systematic understanding and phylogenetic interpretation.

FOSSIL MATERIAL

The first substantial discovery of a Cretaceous mesofossil assemblage containing well-preserved flowers was from fluviatile-lacustrine sediments of late Santonian to early Campanian age at the Åsen locality, Southern Sweden (Friis and Skarby, 1981). Since then many similar floras have been discovered and studied from localities of Cretaceous age in Europe, North America, Central and East Asia, Antarctica, and New Zealand (for references see Friis et al., 2011). The Cretaceous mesofossils occur as isolated organs in unconsolidated clays and sands, and are extracted by sieving in water. Intermediate in size between the larger fossils (macrofossils) that have typically been the focus of Cretaceous paleobotanical research, and fossil pollen and spores (microfossils), the flowers, fruits, seeds and other fossils that comprise mesofossil assemblages rarely exceed more than a few millimeters in length.

Fossil assemblages containing isolated plant fragments are common in Cenozoic strata (e.g, Reid and Reid, 1915; Chandler, 1957; Kirchheimer, 1957; Dorofeev, 1963; Friis, 1985; see also references in Mai, 1995), and have also been obtained from older sediments (Edwards, 1996; Crane and Herendeen, 2009), but several features of many Cretaceous mesofossil assemblages are unusual. In particular, the small size of the individual fossils, and the presence of large numbers of tiny fossil flowers, often with delicate petals, stamens and other floral parts preserved, was completely unanticipated. Also unusual is the abundance of charcoal in these Cretaceous mesofossil assemblages. Comparable assemblages of Cenozoic age, prepared using the same techniques, typically contain fossils with a much wider range of sizes (Tiffney, 1984; Eriksson et al., 2000a), are usually preserved as lignite rather than charcoal, and rarely contain fossil flowers (Friis et al., 2011).

The abundance of charcoal in Cretaceous mesofossil assemblages indicates that natural fires were a major feature of Cretaceous landscapes (Friis et al., 2011; Brown et al., 2012). In the process of charcoalification, the incomplete combustion of plant material under conditions of reduced oxygen resulted in excellent preservation of the 3-D form and cellular detail of diverse plant parts. While some shrinkage of the original plant material often occurs during charcoalification (Harris, 1981; Lupia, 1995), and cell walls are typically homogenized, the shape of the cells is generally more or less unaltered (Scott and Jones, 1991), and very delicate structural details are frequently preserved, as illustrated in the descriptive part of this review. The 3-D preservation of exquisite cellular details, combined with their small size, makes many fossil flowers and other reproductive structures from Cretaceous mesofossil floras especially well-suited for SRXTM. The application of the new technique to charcoalified material has allowed mesofossils to be examined with an unprecedented level of detail and is advancing our understanding of Cretaceous plant diversity in substantial ways.

SRXTM TECHNIQUES

Synchrotron radiation hard X-ray tomographic microscopy (SRXTM) represents a great advance over the application of conventional X-ray approaches in paleontology and has proved a powerful technique for the non-destructive investigation of internal structure in a variety of optically opaque samples. Broadly similar SRXTM techniques can be applied to a wide range of paleobiological material, but here we focus on the techniques used so far for the study of plant mesofossils.

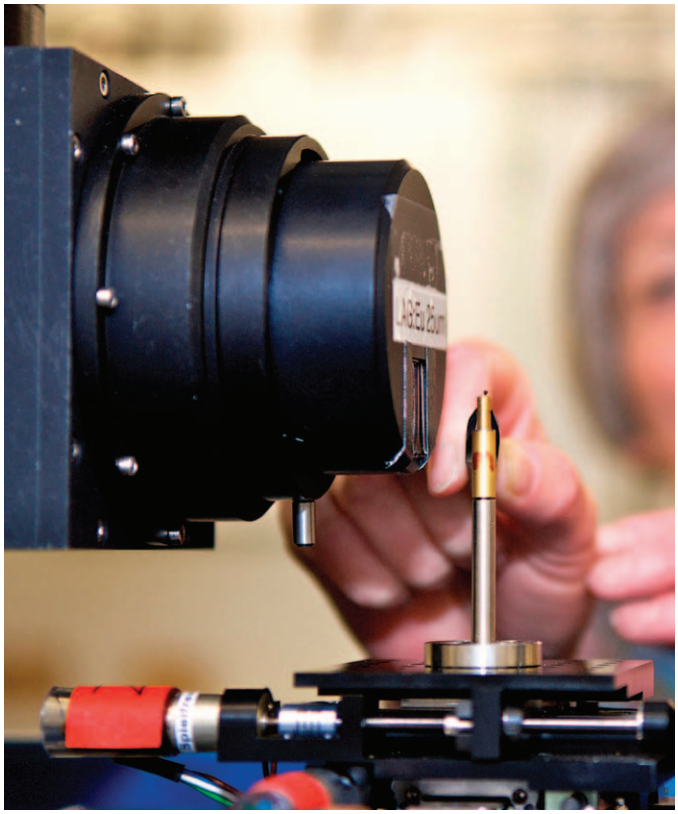

FIGURE 1—Close-up view of the TOMCAT end station showing the sample holder with a fossil flower mounted on a brass stub, 3 mm in diameter, in front of the microscope. (Paul Scherrer Institute photo).

Preparation of plant mesofossils for SRXTM is straightforward. Specimens are analyzed non-destructively and are not altered physically by the process. Unlike SEM no coating is required, and unlike with conventional sectioning of living material dehydrating, fixing or staining of the specimen is not needed. The specimen is usually attached to a support (e.g., a brass pin or SEM stub) with a diameter compatible with that of the beamline sample holder (Fig. 1). Attachment of the specimen to the support is usually done with nail polish for lighter, coalified mesofossils or with wax for heavier, permineralized specimens. Other adhesive typically used for attaching specimens to SEM stubs can also be used. Removal of specimens attached with nail polish can be done easily with a thin blade of a knife, particularly if the contact to the adhesive is small.

The specimens are usually studied also by SEM either prior to or after SXRTM. No additional sample preparation is necessary for investigation of specimens that have previously been coated with gold/platinum and analyzed with SEM. The coating does not obscure internal features. Remounting of specimens from SEM stubs may facilitate reconstruction, but is not a requirement since re-orientation of specimens that have been mounted obliquely can be achieved physically using a goniometer (Mader et al., 2011) or digitally using the reconstruction software (Fig. 2).

Initial examination uses 2-D radiographs taken for different sample orientations using a parallel beam. Photons transmitted through the sample are converted to visible light by a scintillator screen. The image can then be magnified using light microscope optics before being recorded by a digital camera (Fig. 2.1, 2.2). Data from 2-D radiographs provide useful but cumulative

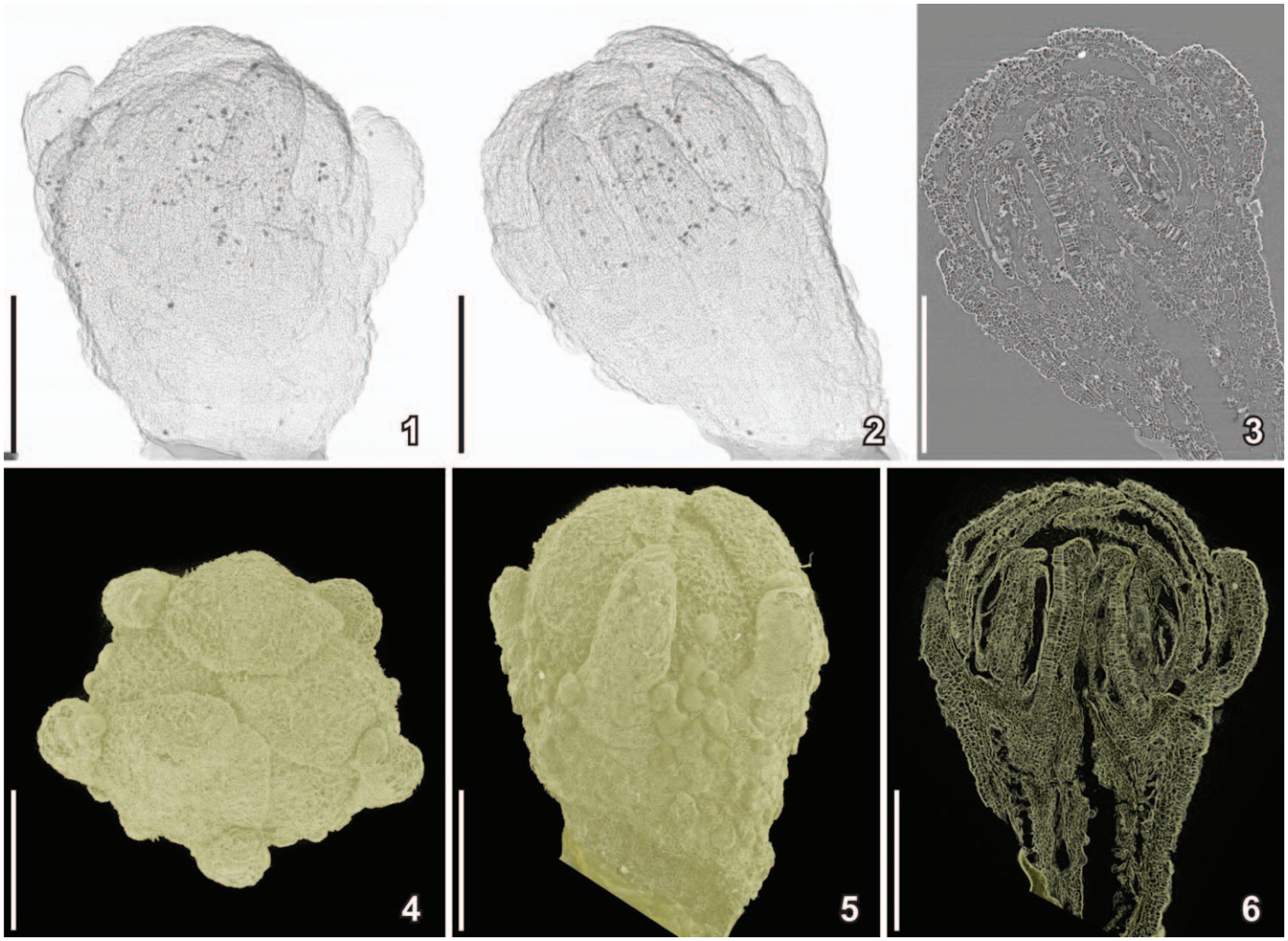

FIGURE 2—SRXTM images of holotype of *Silvianthemum suecicum* (S100376) from the Late Cretaceous Åsen locality, Sweden; dataset acquired using a 10× objective and 20 μm thick LAG:Ce scintillator (voxel size 0.74) at 10 keV; specimen charcoalified and mounted obliquely on SEM stub. *1*, *2*, 2-D dark and flat field corrected radiographic projections for two different sample orientations; *3*, 2-D orthoslice of flower bud in longitudinal view through one style, sample not re-oriented; *4*, *5*, 3-D surface rendering showing external morphology of flower bud in apical and lateral views, respectively; *6*, electronically re-oriented longitudinal section through center of flower bud in 3-D cut voltex (transparent rendering between orthoslices 740–780). Scale bars=500 μm.

information on the internal structure of the specimen along the beam path. However, it is not possible to determine from 2-D projections if a specific feature is located at the front or back of the specimen. To access such 3-D information, a second step requires combining the recorded radiographic dataset (reordered into sinograms) using algorithms based on Fourier analysis (e.g., filtered back-projection) or iterative methods.

SRXTM takes advantage of the absorption and refraction of X-rays during their interaction with matter resulting in different imaging modalities. In absorption contrast tomographic microscopy, X-rays are selectively attenuated as they traverse the sample according to the Beer-Lambert law:

$$I(Z,E)=I_0(E)\exp\left(-\int \mu_l(Z,E)dz\right),$$

where $I(Z,E)$ and $I_0(E)$ are the X-ray beam intensity after and before the specimen. The linear attenuation coefficient $\mu_l(Z,E)$ strongly depends on the atomic number Z: this provides high contrast between materials with different densities, if the X-ray beam energy E is properly selected.

When the analyzed sample is made of light elements, or elements with a similar atomic number Z, contrast is instead obtained by exploiting the refraction of the X-ray beam at material boundaries in the study object and the resulting interference phenomena. The refraction angles are small, but can be determined with great accuracy using phase contrast techniques. The methods commonly deployed in paleontology use the free-space propagation approach (Snigirev et al., 1995; Cloetens et al., 1996). The main advantages with respect to other existing approaches, such as interferometry (Bonse and Hart, 1965; Weitkamp et al., 2005) and analyzer systems (Davis et al., 1995; Chapman et al., 1997) are the high spatial resolution and uncomplicated setup that does not require additional hardware. In the simplest case, pure, so-called, edge-enhancement is exploited by increasing the distance between the sample and the detector. Fresnel fringes are localized at domain boundaries and arise from the interference of the refracted and the directly transmitted beam in case of spatially (partially) coherent radiation. This permits clear visualization of internal boundaries, although the actual contrast between regions with different composition is not improved compared to standard absorption contrast tomography. This technique is routinely used for understanding the internal structure of fossil flowers, fruits, seeds, and other mesofossils.

More advanced approaches enable the extraction of (phase) information coded in the observed Fresnel fringes to further boost the contrast between domains that have similar compositions. The simplest algorithms for phase retrieval (Bronnikov, 2002; Paganin et al., 2002; Groso et al., 2006) work with data acquired at one single sample-detector distance. In this case the setup and protocol is the same as for standard absorption based experiments. These techniques are not fully quantitative and rely on different assumptions, which can often be partially relaxed, but the increased contrast is generally helpful in particularly low absorbing specimens. The concomitant reduction in spatial resolution, which is sometimes observed, can be mitigated by including the high frequency component of the original data.

Fully quantitative, high resolution results (holotomography; Cloetens et al., 1999) can be obtained using datasets acquired at multiple sample-detector distances. Holotomography is, however, rarely used because of the more complicated setup, slower data acquisition and more complex data post-processing that is required.

RECENT DEVELOPMENTS IN SRXTM TECHNIQUES

Spatial resolution.—For parallel beam geometry, the available field of view is determined by the optical configuration chosen and the resolution that is required. In general, the large field of view necessary to accommodate a sample of large volume results in a low magnification dataset whereas higher resolution can be achieved if the field of view is more restricted. For instance, a 20× objective coupled to a sCMOS (scientific complementary metal-oxide-semiconductor) detector provides a pixel size of 0.375 μm across a field of view of 0.85×0.7 mm^2, which is often insufficient for the complete observation of larger specimens at this resolution. When expansion of the available field of view in the direction parallel to the rotation axis is desirable, but high resolution is still required, a stack of several independent tomographic scans can be acquired. However, an increase of the field of view in the direction perpendicular to the rotation axis cannot be obtained by simply juxtaposing single tomographic datasets in this way. Instead it is necessary to merge projections covering the desired field of view laterally prior to tomographic reconstruction.

Although a multi-fold lateral expansion is technically feasible (Haberthür et al., 2010), for most of the mesofossil material examined so far at the SLS a two-fold extension is often sufficient. In such cases, prior to the scan, the rotation axis is positioned at either side of the field of view, rather than in the center, though still ensuring a small overlap for 180° opposed projections. Then, equiangular distributed projections over 360° are acquired. The total number of projections is also increased compared to standard tomographic scans, so as to still satisfy the sampling theorem. Subsequently, projections acquired at an angle θ° and θ°+180° need to be merged, for instance using the overlapping region and a cross-correlation technique, if the exact position of the rotation axis is not known a priori. A single tomographic volume can then be obtained using the merged projections and a standard reconstruction algorithm.

In studies performed so far, high resolution imaging of small fossil flowers with a diameter smaller than 0.7 mm has mostly been accomplished using a 20× objective and a 20 μm thick LAG:Ce (Cerium doped Lutetium Aluminum Garnet) scintillator screen. Specimens as small as 0.3–0.4 mm, as is the case for instance for megaspores, would entirely fit in the field of a 40× objective and could potentially be resolved even more finely providing that the experimental setup is optimized for this purpose. If higher magnification microscope objectives are coupled to thinner scintillator screens, spatial resolution can be pushed to the sub-micron regime even for experimental setups in parallel beam geometry as is shown here for the Cretaceous megaspore *Arcellites* (Fig. 3). The improvement in resolution provided by this configuration is evident (Fig. 3.3). The 2-D slice (Fig. 3.1) was extracted from a tomographic dataset acquired using a 20× objective coupled to a 20 μm thick LAG:Ce scintillator. Comparison with the slices (Fig. 3.2, 3.3) originating from a tomographic volume obtained with a 40× objective and a 5.9 μm thick LSO:Tb (Terbium doped Lutetium Oxyorthosilicate, Lu_2SiO_5) scintillator screen shows clearly the details of the megaspore wall structure, including an outer layer penetrated by narrow, straight canals about 0.4 μm in diameter and 7 μm long. Three-dimensional reconstructions show the spatial distribution of the canals (Fig. 3.4–3.6). Based on these results a new species of *Arcellites* will be established and a detailed description of megaspore morphology and wall structure presented (Friis et al., 2014b). Ongoing optimization of the setup used for the initial acquisition of the data (Fig. 3.2, 3.3) includes improvement of the scintillator screen positioning system, ensuring homogeneous focus across the entire field of view, and a pre-processing alignment step to correct for any possible mechanical vibrations or imperfections in the rotation that would lower resolution.

Density resolution.—During the past few years, microtomography end-stations at third generation synchrotron sources have been optimized in important ways resulting in datasets of astonishing quality. In early applications of SRXTM to coalified Cretaceous mesofossils, phase retrieval approaches were often necessary to achieve the desired resolution (Friis et al., 2007). However, now, simple absorption contrast is often sufficient. New developments in detector technology (e.g., sCMOS), as well as improvements in scintillating materials, have significantly improved the signal-to-noise ratio in tomographic datasets and resulted in improved density resolution. These developments have also enhanced the efficiency of the tomography setup, reducing the time necessary for the acquisition of a high-resolution scan by approximately a factor of 20. This improvement in efficiency enables the acquisition protocol to be optimized (e.g., increased number of projections, frame-averaging) to boost signal-to-noise ratio and ultimately density resolution. When applied to these highest quality tomographic datasets, new phase retrieval algorithms permit density resolution to be pushed even further.

Efficient data acquisition and increased computing power also allows the complementarity of absorption and phase contrast tomographic microscopy (spatial resolving power vs. density resolving power) to be easily exploited. A single specimen can be readily examined using both absorption and phase contrast tomographic microscopy. For small, low absorbing samples (1 mm in diameter or smaller), such as many Cretaceous flowers, it is generally sufficient to acquire one tomographic dataset with the object positioned as close to the microscope as mechanically allowed by the setup (typically at least 5 mm). From these data two different tomographic volumes can be reconstructed.

Projections can be reconstructed using algorithms for absorption-based tomography providing the 3-D distribution of the X-ray linear attenuation coefficient with edge-enhancement. Despite little contrast due to the small difference in the linear attenuation coefficient between air and the specimen, datasets reconstructed in this way are characterized by high resolution and sharp edges. Alternatively, information coded in the Fresnel fringes in the same projections can be unraveled by phase retrieval approaches prior to tomographic reconstruction to yield the 3-D distribution of the pseudo-phase information (compare Fig. 3.2, 3.3). In this case the results are generally not truly quantitative, and phase contrast tomographic volumes often have lower resolution, but the boosted contrast is useful to differentiate among domains with similar compositions. Both approaches have inherent

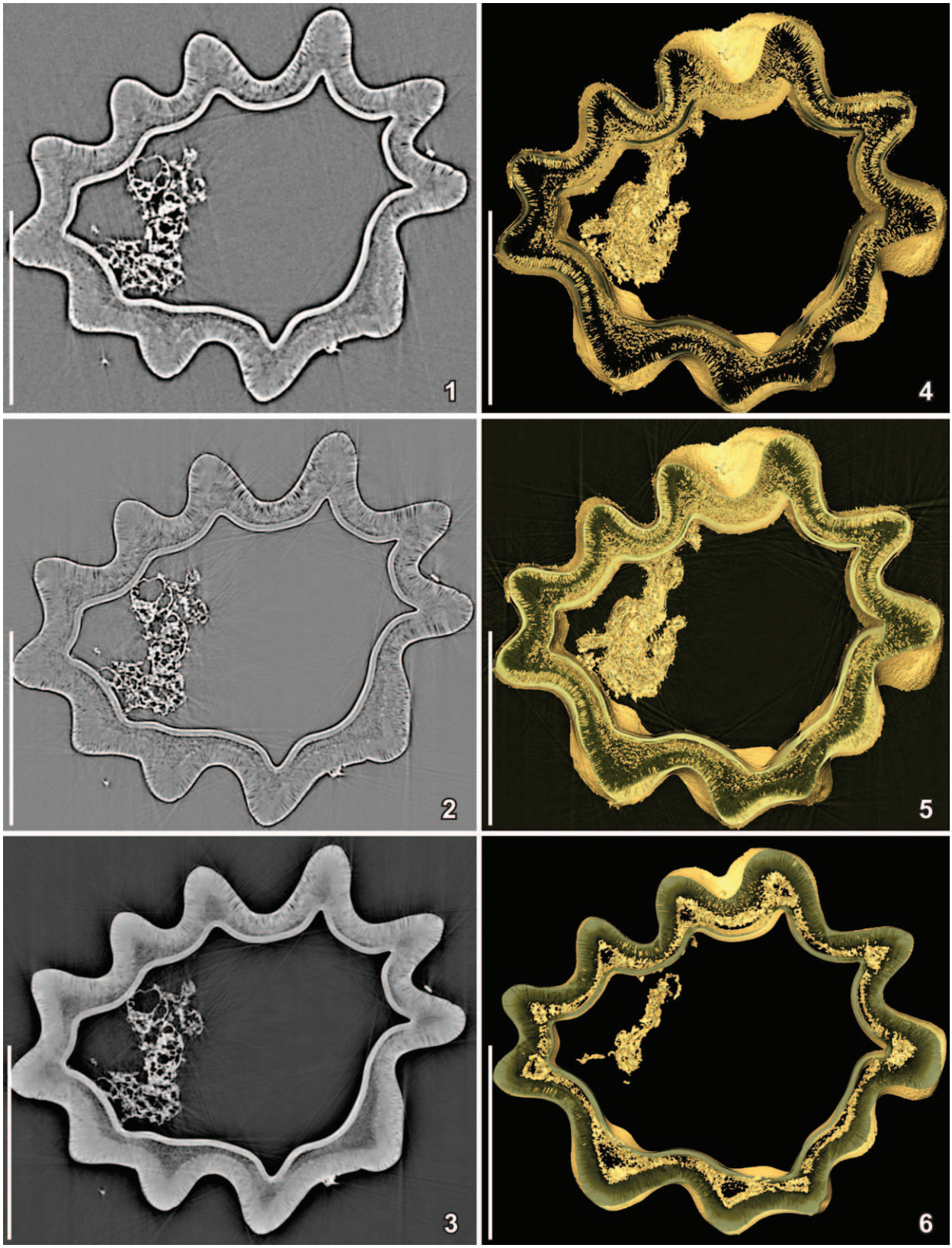

FIGURE 3—SRXTM images of the megaspore *Arcellites* sp. (S171531) from the Early Cretaceous Torres Vedras locality, Portugal; dataset acquired using a 20× objective and 20 μm thick LAG:Ce scintillator (voxel size 0.37) at 10 keV (*1*) and a 40× objective with a 5.9 μm thick LSO:Tb scintillator (voxel size 0.1625) at 10 keV (*2–6*); images in *1*, *2* and *4*, *5* have been reconstructed uniquely exploiting absorption contrast and pure edge-enhancement. Images in *3*, *6* were obtained using simple phase retrieval (Paganin et al., 2002), but with the subsequent addition of the high frequency component of the original data to minimize loss in spatial resolution inherent in phase retrieval. *1–3*, 2-D reconstructions of a transverse section through the body of the megaspore showing wall ultrastructure composed of a thin inner, almost solid, uniform layer, a middle granular-fibrous layer of uneven thickness, and an outer layer penetrated by very fine canals; note difference in resolution between *1* originating from a tomographic volume obtained with a 20× objective and a 20 μm thick LAG:Ce screen, and

shortcomings, but techniques for fusing and integrating the information provided by the different contrasts are also being developed.

Image quality and artifact reduction.—Even with careful attention to both experimental and post-processing procedures, image artifacts can occasionally reduce the quality of the results obtained. For example, despite using adequate scanning protocols, high quality scintillators and digital cameras it is difficult to completely avoid rings, one of the most common class of artifacts in reconstructed tomographic slices. Rings can have different causes. Sharp rings arise from dead pixels in camera chips and damaged and dirty scintillators, whereas wide and faint rings are the result of synchrotron beam instabilities.

A suite of algorithms for the mitigation of rings and other artifacts are continuously being developed and several software routines based on different approaches (Sijbers and Postnovz, 2004; Boin and Haibel, 2006; Titarenko et al., 2010) are available for clearing such artifacts from reconstructed slices. A fast and stable method (Münch et al., 2009), which makes use of a combined wavelet-FFT decomposition of the sinogram prior to tomographic reconstruction, has proven particularly helpful for clearing such artifacts from the specimens. A high degree of separation of the artifacts from the true image signal, as well as the strict condensation of the artifacts into a few coefficients of the decomposed sinogram, is achieved by this technique. This enables highly selective filtering of the unwanted features with only marginal perturbations of the true image information yielding data of astonishing quality.

High-resolution visualization and quantification of small parts of larger samples is sometimes needed. Local tomography acquisition schemes can deliver this information without need for lateral extension of the field of view and therefore a more sophisticated and time-consuming acquisition protocol. However, this approach often results in artifacts (significant overestimation of the attenuation coefficients in the proximity of the reconstruction circle and cupping artifacts). This greatly reduces the portion of the slice that can actually be evaluated and makes segmentation and quantitative analysis difficult. To mitigate such problems the reconstruction approach needs to take into account the incompleteness of the projection data. Artificial lateral extension of the sinogram prior to reconstruction with the aim of simulating the missing data significantly reduces typical local tomography artifacts. The most straightforward approach calls for lateral padding of the sinogram on both sides with the values in its first (for the left side) and last (for the right side) column (Marone et al., 2010). The quality improvements provided by this simple procedure are striking. Significant overestimation of the attenuation coefficients in the proximity of the reconstruction circle is eliminated and the cupping artifact is strongly reduced. To attenuate the remaining artifacts, more complicated algorithms are needed, for example, involving a wavelet-based multiresolution approach (Rashid-Farrokhi et al., 1997).

Serious streaking artifacts often result from photon starvation, when insufficient photons are reaching the detector. This artifact is typically seen in low absorbing specimens that also contain few high absorbing domains. To achieve maximum contrast within the low attenuating part of the sample, the energy of the X-ray beam is often optimized for those regions. However, X-rays passing near or through the strongly absorbing parts are often highly attenuated and therefore the corresponding areas on the projections are more strongly contaminated by noise. If standard analytic techniques (Kak and Slaney, 2001; Marone and Stampanoni, 2012) are used for the tomographic reconstruction, bright streaks radiating from the high absorbing particles are observed. This occurs because the reconstruction process assumes that each detector measurement is equally accurate and it magnifies the noise in the absence of advanced noise regularization. Streak artifacts occur commonly in mesofossils in which pyrite (high-absorbing) has formed during preservation. Among the Cretaceous mesofossils that we have examined this is particularly pronounced in specimens from near-coastal deposits at the Late Cretaceous Mira locality in Portugal (Fig. 4.5). However, pyrite, and sometimes fluorite from mesofossils that have not been rinsed sufficiently during extraction and cleaning, may cause problems in specimens from other samples as well. Reconstruction approaches that are being developed in the medical field to overcome scan deterioration when a metal implant cannot be avoided (Prell et al., 2010; Boas and Fleischmann, 2011) may be helpful in these cases. Such techniques, the most advanced of which are based on iterative procedures, should also prove adequate to handle paleontological specimens contaminated by pyrite without the need for an energy increase and therefore some loss of contrast.

SRXTM COMPARED TO LABORATORY X-RAY SOURCES

The very significant photon density reached by third generation synchrotrons brings huge advantages compared to traditional X-ray laboratory sources, especially when exceptional spatial, temporal and density resolution is required. The high brilliance of synchrotron light allows increased spatial and temporal resolution, including the routine and rapid detection of details as small as 1 μm in millimeter-sized samples. Throughput times of only a few minutes also permit a large amount of material to be scrutinized in a short time enabling the selection of the most significant and best-preserved specimens for more detailed analysis. The monochromaticity of the X-ray beam also enables quantitative measurements of material properties and easier identification of different phases, if the radiation energy is properly tuned, since beam hardening artifacts, which are often characteristic of laboratory X-ray sources, can be avoided. The unique monochromaticity and high photon flux of synchrotron radiation results in images with increased contrast and reduced noise. Results are also enhanced by the absence of cone beam artifacts thanks to the almost parallel beam geometry typical at tomographic microscopy end-stations at synchrotron sources. Unlike laboratory based X-ray CT, the coherence of synchrotron light allows SRXTM to exploit both absorption and phase contrast imaging, enabling optimal investigation of both low- and high-absorbing samples.

SEM COMPARED TO X-RAY APPROACHES

In SEM the signal is the result of the interaction of the electron beam with atoms at or near the surface of the sample. In the most common or standard detection mode, secondary electrons are measured. Since the yield of secondary electrons depends on the angle of incidence between the beam and the specimen surface, and since this angle varies because of the local inclination of the specimen, SEM produces characteristic

←
2 and *3* originating from a tomographic volume obtained with a 40× objective and a 5.9 μm thick LSO:Tb screen; *4–6*, 3-D reconstructions combining cut voltex and isosurface rendering with different thickness of sections and different color intensities to enhance the spatial distribution of canals in the outer layer showing concentration of the canals between the ridges of the wall (*4*, *5*) and the uneven distribution of the granular-fibrous material that makes up the middle layer (*5*, *6*). Scale bars=100 μm.

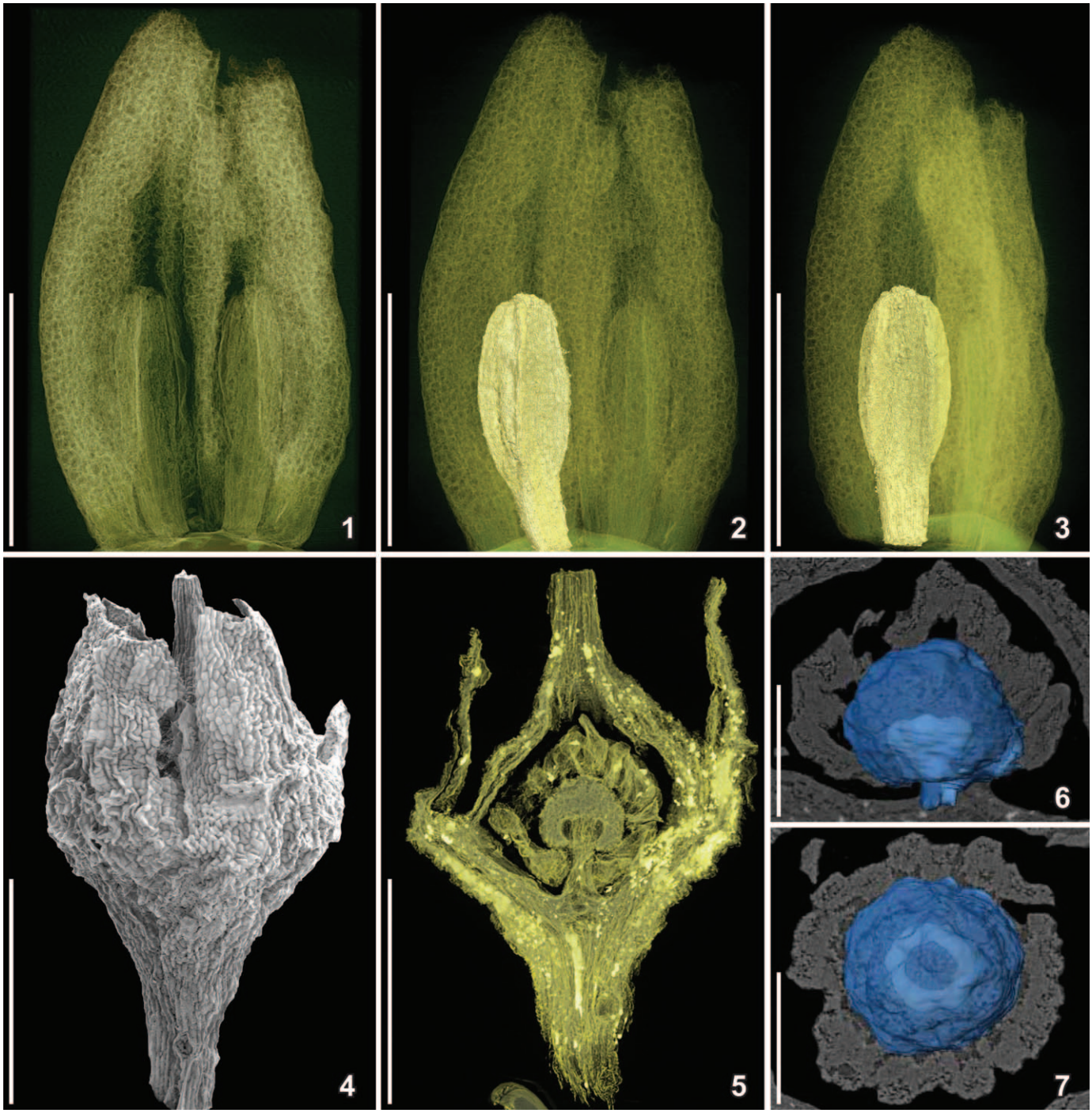

FIGURE 4—SRXTM reconstructions (*1–3*, *5–7*) and SEM image (*4*) of charcoalified fossil flowers from the Early (*1–3*) and Late (4–7) Cretaceous of Portugal showing volume rendering and voltex reconstructions of floral parts; *1–3*, fragments of unnamed pentamerous fossil flower (S171526) from the Early Cretaceous Catefica locality, Portugal, showing two bulky tepals, each almost completely enveloping a stamen; the thick transparent voltex section (*1*) and the surface renderings embedded in the voltex reconstruction (*2*, *3*) show the extensive development of the connective between the small pollen sacs and gradual transition from the bulky filament into the basifixed anther; dataset acquired using 20× objective and a 20 μm thick LAG:Ce scintillator at 10 keV (voxel size 0.37); *4–7*, unnamed primuloid flower from the Late Cretaceous Mira locality, Portugal; *4*, external morphology of flower (S170155); *5*, 3-D SRXTM reconstruction of same flower in *4;* cut voltex section (transparent rendering between orthoslices 570–660) showing the mushroom-shaped placenta in longitudinal section bearing tiny, densely crowded ovules; pyrite infilling in the tissues is seen as lighter yellow regions; dataset acquired using 10× objective and a 20 μm thick LAG:Ce scintillator at 12 keV (voxel size 0.74); *6*, *7*, 3-D SRXTM reconstruction of placenta region of flower (S153146) in lateral (*6*) and apical (*7*) view superimposed on phase retrieved orthoslices; dataset acquired using 10× objective and a 20 μm thick YAG:Ce scintillator at 10 keV (voxel size 0.74 μm). Scale bars for *1–5*=500 μm; for *6, 7*=150 μm.

3-D topographic contrast. This enables morphology of the sample surface to be imaged, revealing details less than 1 nm in size. However, while SEM can provide high-resolution morphological details, it provides no information on the internal structure of specimens, unless they can be sectioned or the specimens are fragmented. Chemical information can be obtained, if the back-scattered secondary electrons (BSE) are detected, since their signal is strongly related to the atomic

number, but in all cases, the information retrieved from SEM studies is limited to data from the surface of the specimen.

In contrast to SEM approaches, the potential of hard X-rays for the non-invasive investigation of the interior of fossil material has long been recognized. Their depth of penetration has been widely exploited in paleontology. Initial efforts using X-rays were limited in their resolution, but new approaches using SRXTM provide both high penetration and high resolution to reveal fine details of internal structure. Volume renderings of SRXTM datasets can also provide detailed surface information independent of the angle from which the specimen is viewed, enabling the direct correlation of internal and surficial features.

APPLICATION OF SRXTM TECHNIQUES TO CRETACEOUS FOSSIL PLANTS

To fully understand the structure and organization of fossil flowers and other mesofossils it is necessary to study both external and internal features. In the case of flowers that are open (anthetic) external morphology and the general position of floral parts, and their number, can often be studied using SEM alone, especially when multiple specimens are available. However, in flower buds critical features, such as structure and organization of stamens and carpels, are concealed. Similarly, information on vasculature in the floral organs, placentation, number and position of ovules, and ovule organization is also unavailable from external examination unless some specimens are fragmented or can be sacrificed to fracturing or sectioning for internal examination.

In several studies of Cretaceous flowers, embedding in resin or other hard material followed by conventional serial sectioning using an ultramicrotome has been applied to reveal the internal features in a more precise way than is possible by fracturing specimens. Good results were obtained for *Scandianthus costatus* Friis and Skarby (1982), *Silvianthemum suecicum* Friis (1990), *Mauldinia mirabilis* Drinnan et al., (1990), *Mauldinia angustiloba* Viehofer et al., (2008), *Esgueiria adenocarpa* Friis et al., (1992), *Normanthus miraensis* Schönenberger et al., (2001b), *Paradinandra suecica* Schönenberger and Friis (2001), *Platydiscus peltatus* Schönenberger et al. (2001a), and *Endressianthus miraensis* Friis et al., (2003). However, sectioning is not always successful. Complete penetration of the embedding material into the specimens is sometimes difficult to achieve, and the brittle nature of charcoalified material means that cells are often crushed during sectioning. The small size of the specimens also means that sections can be made only in one direction and these one-directional sections are not always straightforward to interpret.

A further problem with conventional sectioning is that many critical fossils are unique, for instance with a type specimen (e.g., holotype of *Silvianthemum suecicum*; Fig. 2) or where there is only one specimen of a taxon (e.g., holotype and only specimen of *Monetianthus mirus* Friis et al., 2009; Fig. 5). Even a taxon represented by numerous specimens may include one or a few of those specimens that are especially valuable because they are preserved differently and show different features (e.g., *Scandianthus costatus*; Figs. 7, 8), or because they represent a certain ontogenetic/developmental stage, such as a closed flower bud, an anthetic flower with floral organs preserved or a mature fruit with seeds. In other cases fossils with similar morphology can only be distinguished by internal features, such as the *Canrightia*-complex (Fig. 6).

For these reasons the recent development of non-destructive SRXTM techniques is of the utmost importance for advancing the study of the Cretaceous mesofossils. SRXTM allows investigation of external and internal features at high resolution, provides 3-D reconstructions, allows 2-D sections of the same specimen to be prepared in all directions and creates the possibility of virtual dissections. Specimens require no special preparation and because many specimens can be imaged rapidly SRXTM also allows a collection of many specimens to be screened for certain features or for the quality of their preservation.

Reconstructions and virtual sections shown here were made using Amira or Avizo software, but there are several other tools for assembling and visualizing the digital datasets amassed from the SRXTM analyses. Sections can be a single pixel thick 2-D slice, which is often necessary for studying cellular or structural details (Figs. 2.3, 3.1–3.3, 6.4, 6.5, 7.4–7.6, 8.7–8.9, 9.3, 9.6), but some features are better studied in thicker sections that mimic conventional serial sections in being thicker and in having a 3-D component. This can be done by merging several consecutive slices and using transparent voltex reconstructions (Figs. 2.6, 4.1, 4.5, 8.1–8.4, 9.1, 9.4, 9.5, 10.4–10.6) or a combination of voltex and isosurface reconstruction (Figs. 3.4–3.6, 5.4–5.6, 6.3).

It is also possible to understand the morphology of individual internal organs or tissues by rendering selected surfaces or sections of the fossils. This can be time consuming, but may be particularly helpful for complex structures. We illustrate here surface renderings of a stamen in an Early Cretaceous flower from the Catefica locality (Fig. 4.2, 4.3) and of the placenta in a Late Cretaceous flower from the Mira locality (Fig. 4.6, 4.7). Because, the stamen was partly free from other tissues the rendering of this structure was relatively straightforward and could be performed within a day. Rendering of the placenta was performed in a couple of days. Rendering of more complex structures, such as the vasculature in *Monetianthus* (Friis et al., 2009b), is more time consuming and may take several days to complete. The Catefica flower shows typical Early Cretaceous angiosperm stamens with extensive development of the connective between the small pollen sacs and gradual transition from the bulky filament into the basifixed anther. The Mira flower shows an unusual mushroom shaped placenta that along with other features suggests a systematic position close to the *Primula*-group among extant Ericales (Friis et al., 2010).

In addition, because an important part of understanding of the organization and structure of plant fossils is careful comparison with comparable structures in putatively closely related extant plants, SRXTM can be used to study preserved material of living plants to provide direct comparison with fossil material. Morphological and histological details of extant plants are not always described at the level of detail for which the fossil material is understood. The application of SRXTM to dehydrated (critical point dried) extant flowers reveals excellent cellular details and possibilities for spatial reconstruction, for example as in the comparative study of extant *Quintinia quatrefagesii* F. Muell (Fig. 9.1–9.3) with fossil *Bertilanthus scanicus* Friis and Pedersen (2012) and *Silvianthemum suecicum* (Fig. 9.4–9.6) (Friis et al., 2013b).

Monetianthus mirus*: the recognition of Nymphaeales in the Early Cretaceous*.—*Monetianthus mirus* from the Early Cretaceous Vale de Agua locality in western Portugal exemplifies a fossil taxon that is represented only by a single, fragmentary specimen. The fossil is lignitized, slightly compressed and has lost all perianth parts and stamens leaving only scars from these organs on the surface of the fossil (Fig. 5.1, 5.2). A characteristic feature of the fossil is the presence of a central protrusion in the flower surrounded by the gynoecium. This together with the many carpels and other floral parts strongly suggested relationship with extant Nymphaeales (Friis et al., 2001). The systematic assignment was later questioned by Gandolfo et al. (2004), who

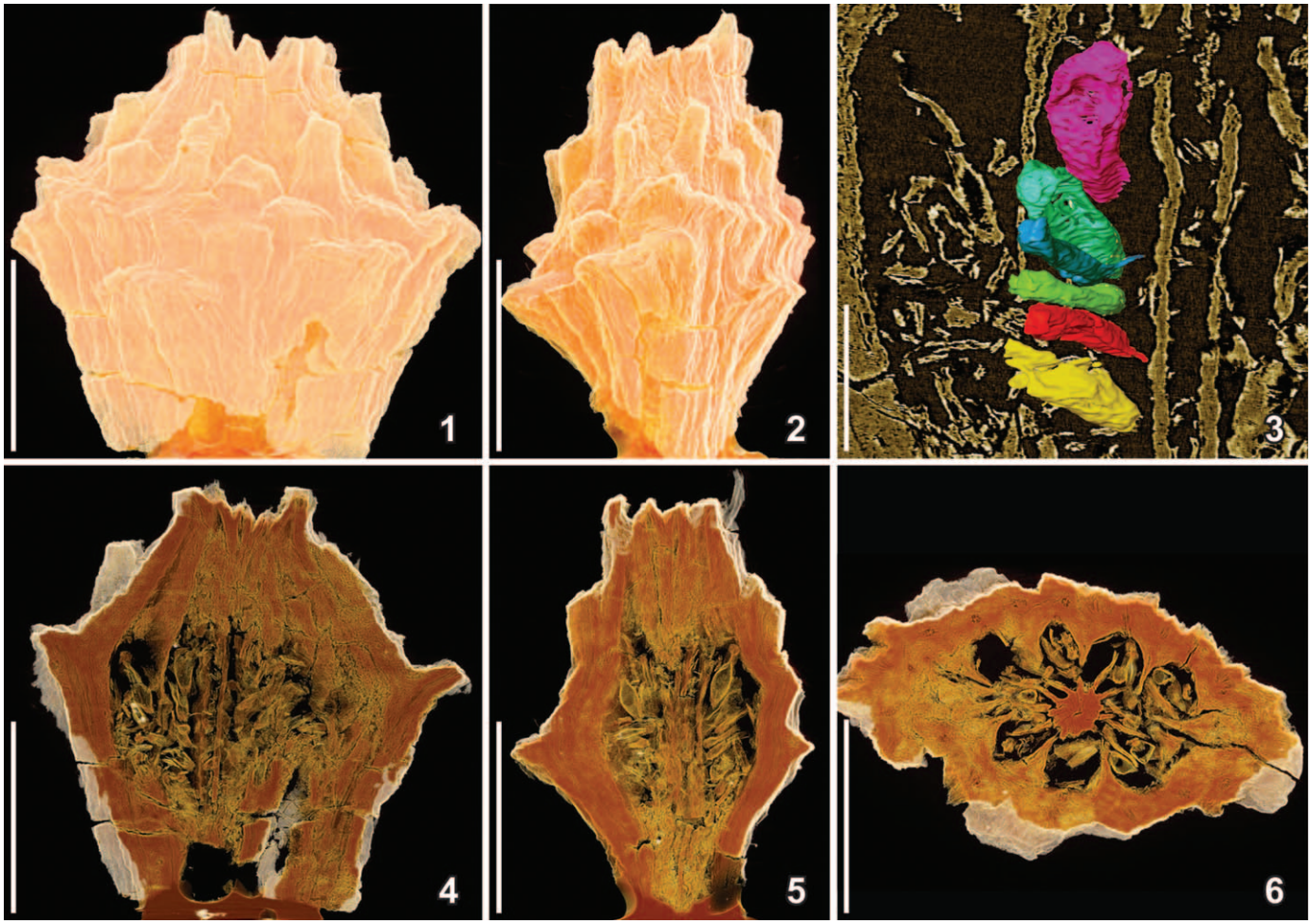

FIGURE 5—Three-dimensional (*1*, *2*, *4–6*) and 2-D (*3*) SRXTM reconstructions of the lignitized flower *Monetianthus mirus* (S122015) from the Early Cretaceous Vale de Agua locality, Portugal; dataset acquired using 4× objective and a 20 μm thick YAG:Ce scintillator at 10 keV (voltex size 1.85 μm); specimen gold coated and studied by SEM prior to the SRXTM analysis; manipulation with Avizo software highlight the gold cover that has higher density than the coalified tissue; *1*, *2*, 3-D surface rendering of fossil in two different lateral views showing scars from perianth and androecium; *3*, 3-D surface rendering of selected ovules superimposed on an 2-D orthoslice showing anatropous ovules with thin funicles directed towards the septum (laminar placentation); *4–6*, 3-D reconstructions combining cut voltex (transparent rendering) and surface rendering of fossil in two different lateral views (*4*, *5*) and in apical view (*6*) showing syncarpous ovary with many small ovules that do not fill the ovary cavity, section in *4* between orthoslices yz380 and 320, section in *5* between orthoslices xz720–750 and section in *6* between xy620–670. Scale bars for *1*, *2*, *4–6*=500 μm; for *3*=250 μm.

instead suggested relationship with extant *Illicium* L. (Schisandraceae), in which the flowers also have many carpels surrounding a central protrusion.

Flowers of *Illicium* differ from those of the Nymphaeales in having a single median ovule per carpel in contrast to two or, more commonly, numerous, non-median ovules in Nymphaeales. Also, in *Illicium* the single ovule fills out the whole ovary cavity while in Nymphaeales this is not the case. A further important distinguishing feature is the presence of laminar placentation in Nymphaeales, a feature that is generally very rare among extant angiosperms, and is known outside the Nymphaeales only for the monocot order Alismales. Extant members of Schisandraceae have axile placentation.

In the single specimen of *Monetianthus mirus* several key features of the gynoecium were not visible from the outside. A small piece was broken from the base of the ovary in the hope of discerning internal organization and structures. This made it possible to see more ovules inside the fossil, but their number and placentation could not be observed. The application of SRXTM was therefore critical for accurately describing and analyzing this unique specimen (Friis et al., 2009b). The fossil specimen was heavily gold-coated after it had been remounted on the SEM stub several times to observe the morphology from different sides. The coating is visible in the SRXTM images (Fig. 5.1, 5.2, 5.4–5.6), but does not obscure or disrupt examination of internal features. SRXTM unequivocally demonstrated several ovules, about 0.3 mm long, per carpel (Fig. 5.3–5.6). SRXTM analyses also clearly show laminar placentation with the ovules borne on the septa in an ascending position (Fig. 5.3). It is also clear that ovules are not in contact with the ovary wall and do not fill out the ovary cavity (Fig. 5.4–5.6) as they do in *Illicium*. These characters confirmed the earlier placement of the fossil flower in the Nymphaeales and *Monetianthus mirus* remains the oldest well-documented floral record of this basal lineage of angiosperms.

Carpestella lacunata von Balthazar et al. (2008) from the Early Cretaceous Puddledock locality, Virginia, is another mesofossil represented by a single specimen in which SRXTM has been critical for clarifying internal structures and organization. Like *Monetianthus mirus Carpestella lacunata* is preserved with the perianth and androecium represented only by theirs scars. *Carpestella lacunata* has 13 carpels arranged around a central protrusion, similar to the organization in *Monetianthus mirus*, but

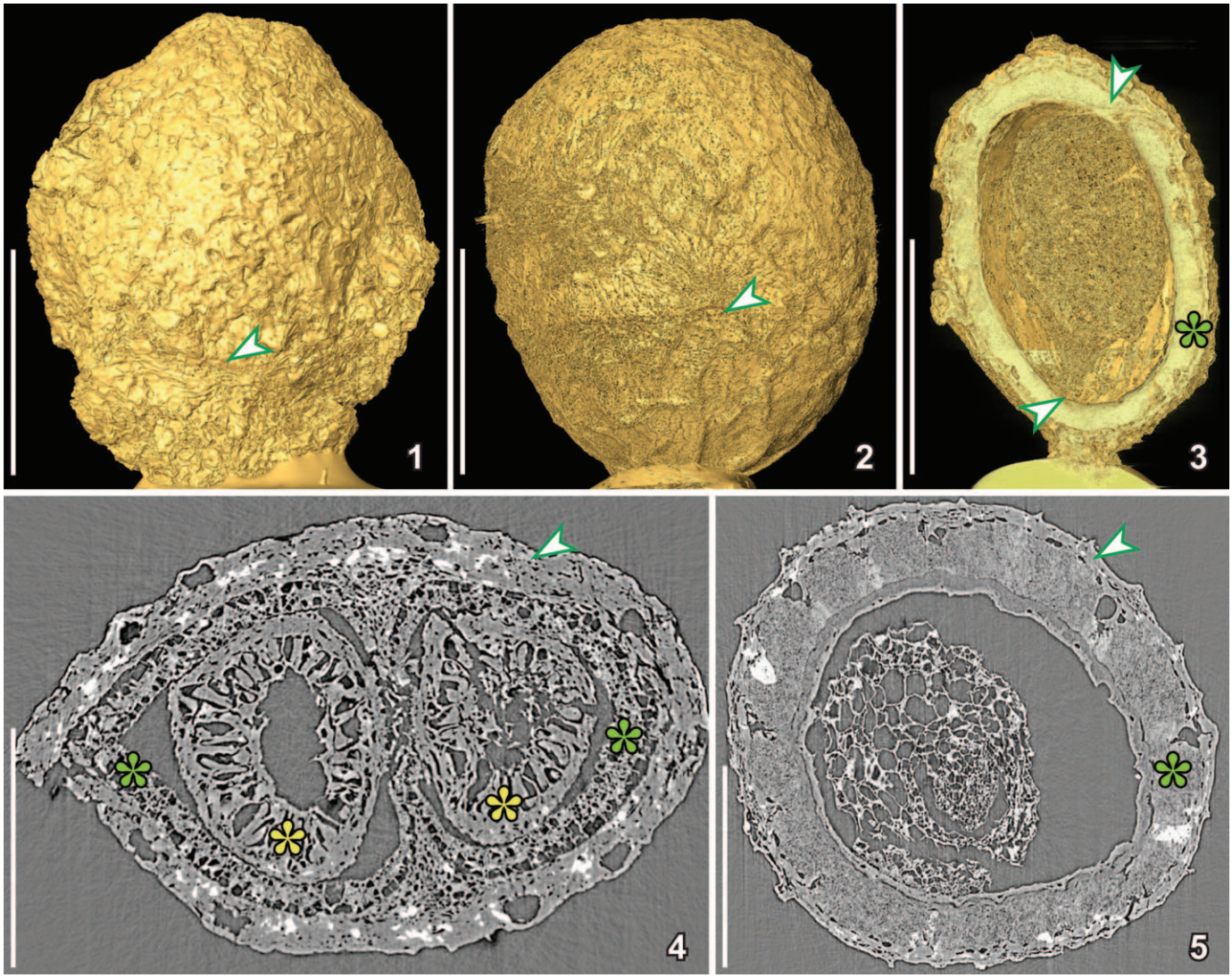

FIGURE 6—Three-dimensional (*1–3*) and 2-D (*4*, *5*) SRXTM reconstructions of two charcoalified fruits with similar external morphology, but different internal structure; *1*, surface rendering of *Canrightia resinifera* (S171508) from the Early Cretaceous Catefica locality, Portugal, showing slightly wrinkled surface of fleshy fruit wall and short hypanthium (arrowhead); dataset acquired using 10× objective and a 20 μm thick LAG:Ce scintillator at 10 keV (voxel size 0.74 μm); *2*, surface rendering of *Canrightia*-like fruit (S174033) from the Early Cretaceous Famalicão locality, Portugal, showing slightly wrinkled surface of fleshy fruit wall and scars from stamens (arrowhead) on the fruit surface; dataset acquired using 20× objective and a 20 μm thick LAG:Ce scintillator at 10 keV (voxel size 0.325 μm); *3*, combined surface rendering and cut voltex (transparent rendering) of *Canrightia*-like fruit (S174105) from the Early Cretaceous Buarcos locality, Portugal, in longitudinal section showing a single, hemi-orthotropous and pendulous seed with chalaza and vascular bundles entering the seed close to apex (arrowhead) and micropyle directed towards the base (arrowhead) and with thick crystalliferous endotesta (green asterisk); dataset acquired using 20× objective and a 20 μm thick LAG:Ce scintillator at 10 keV (voxel size 0.325 μm); *4*, transverse orthoslice of *Canrightia resinifera* (same dataset as for *1*) showing fruit wall (arrowhead) enclosing two ovules/seeds with the seed wall composed of crystalliferous and fibrous endotesta (green asterisks) and a thick endotegmen composed mainly of endothelium cells (yellow asterisks); *5*, transverse orthoslice of *Canrightia*-like fruit with collapsed fruit wall (arrowhead) enclosing a single seed (same dataset as for *2*); seed wall mainly composed of crystalliferous and fibrous endotesta and with grooves giving the seed surface a pitted appearance; inside are remains of endosperm and embryo. Scale bars for *1–3*=500 μm; for *4*, *5*=250 μm.

information on ovules and placentation is uncertain. Although most features indicate affinity with Nymphaeales the systematic position of *Carpestella lacunata* is not fully resolved (von Balthazar et al., 2008).

The early presence of the Nymphaeales in angiosperm diversification is supported by macrofossil occurrences such as the compression fossils of *Pluricarpellatia peltata* B. Mohr, Bernardes-de-Oliveira and David W. Taylor (2008) from the Early Cretaceous of Brazil. There is also convincing evidence from fossil seeds that the Nymphaeales had undergone considerable diversification by the mid-Early Cretaceous. Nymphaealean seeds are characterized by their exotestal organization, presence of a micropylar lid and palisade-shaped exotestal cells with strongly wavy anticlinal cell walls (Friis et al., 1999, 2000, 2010, 2011). Examination of a series of exotestal seeds with these features from Early Cretaceous sediments using SRXTM is currently helping to understand the full diversity present among this complex of seeds and is revealing great diversity in cell form and internal structure. Preservation is typically good and sometimes superb with delicate cells of endosperm and embryo-tissue preserved. Further examination of this material may help unravel important aspects of early evolutionary innovation in angiosperm ovules and seeds.

Canrightia resinifera *Friis and Pedersen (2011) and other Early Cretaceous angiosperms: early diverging lineages from the main branch of the angiosperm phylogenetic tree*.—Early

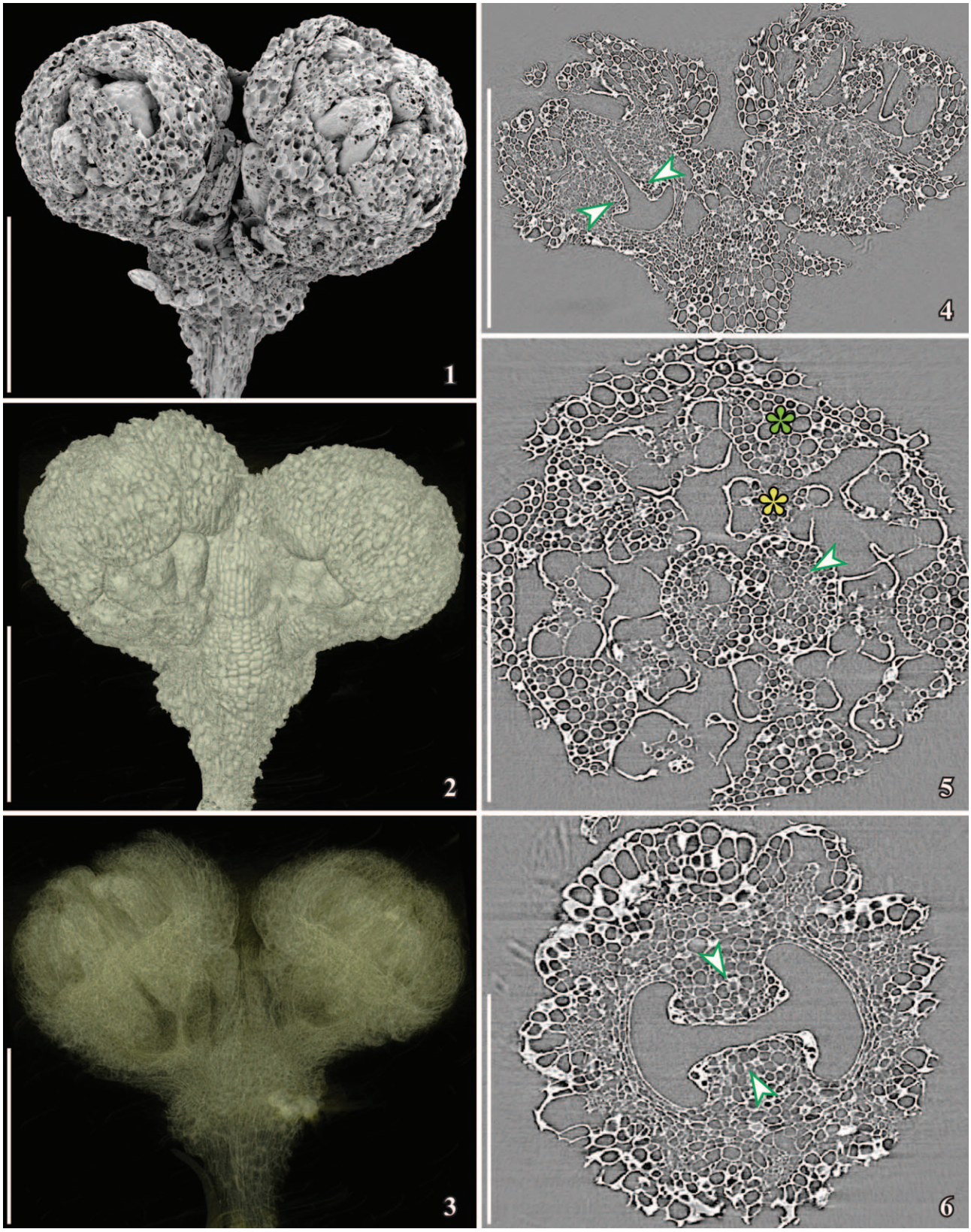

FIGURE 7—SEM image (*1*), 3-D (*2*, *3*), and 2-D (*4–6*) SRXTM reconstructions of two charcoalified flower buds of *Scandianthus costatus* (S172382) from the Late Cretaceous Åsen locality, Sweden; dataset acquired using 10× objective and a 20 μm thick LAG:Ce scintillator at 10 keV (voxel size 0.74 μm); *1*, morphology of flower buds showing slightly worn surface; *2*, SRXTM volume rendering showing flower buds and supporting bract (viewed from the opposite direction to that in *1*); *3*, voltex reconstruction (transparent rendering) of same view as in *1*; *4*, longitudinal orthoslice through central part of flowers showing apical placentae (arrowheads) in left flower; *5*, transverse orthoslice showing, from the outside toward the center, remains of three sepals, a whorl of five bulky petals (one marked with green asterisk), two whorls of five stamens (one marked with yellow asterisk), each stamen with two pairs of pollen sacs, and in the center two free styles (arrowhead); *6*, transverse orthoslice through the ovary showing the two apical placentae (arrowheads); ovules are not developed in this very young flower bud. Scale bars for *1–4*=500 μm; for *5*, *6*=250 μm.

Cretaceous mesofossil assemblages from Portugal include a large number of small oval to spherical fruits, typically 1–2 mm long. Most of these are apparently unicarpellate and many are berries or drupes with a fleshy fruit wall (Eriksson et al., 2000b). The fruit wall is often wrinkled and there are few external features that can be used to distinguish these fossils (Fig. 6.1, 6.2). Screening of many specimens using SRXTM has revealed that these small, superficially uniform fruiting structures include a rich diversity of forms distinguished by the number of ovules/seeds as well as their orientation and organization, which could not have been discerned from studies of external features alone.

Fossil floral structures and fruits of the extinct species *Canrightia resinifera* belong to this complex of fossils (Fig. 6.1, 6.4). *Canrightia* Friis and Pedersen (2011) occurs commonly among the Early Cretaceous mesofossil floras from Portugal and is particularly abundant in the mesofossil assemblage from Famalicão (Friis and Pedersen, 2011). Rare specimens with well-preserved floral organs show that flowers of *Canrightia* were bisexual and apparently radially symmetrical with a single whorl of tepals in a perigynous position, each opposite and closely associated with a single bulky stamen. The ovary is semi-inferior, apparently symcarpous with two to five hemi-orthotropous, bitegmic and pendant ovules. Differences in preservation between fossils from the different localities sometimes make identification difficult, but SRXTM has revealed several features of the gynoecium that unite fossils from the different localities. Ovules are endotestal-endotegmic with a distinct crystalliferous and fibrous infilling of the endotestal cells and distinctive endothecial cells in the endotegmen (Fig. 6.4).

Phylogenetic analysis suggests a position for *Canrightia* close to the root of the eumagnoliid tree (Friis and Pedersen, 2011). There are particularly strong similarities to extant Chloranthaceae and also to some Piperales. Both *Canrightia* and extant Chloranthaceae have orthotropous and pendant ovules with endotestal organization and a distinct crystalliferous endotesta. *Canrightia* differs, however, from Chloranthaceae in having more than one ovule per ovary. The endotegmen with a prominent endothelium that characterizes the ovules of *Canrightia* is also not seen in Chloranthaceae. A very similar endothelium is, however, present in Lactoridaceae (Piperales). Flowers of Chloranthaceae are distinguished from those of *Canrightia* and most Piperales in being monosymmetrical.

A newly identified fossil taxon from the Early Cretaceous of Portugal has ovules/fruits very similar to those of *Canrightia*. This material may bridge part of the gap between *Canrightia* and extant Chloranthaceae. The new fossil is known from an extensive collection of small unicarpellate and fleshy fruits (Fig. 6.2, 6.3, 6.5). Scars on the surface of the fruits indicate the same floral organization as in *Canrightia*, but the perianth is lacking as in extant Chloranthaceae and the only indications of a perigynous hypanthium are scars from stamens about one third of the way from the base on the fruit surface, as also occurs in extant *Chloranthus* and *Sarcandra*. SRXTM shows that the ovary of the new species has only a single ovule (Fig. 6.3, 6.5), as in extant Chloranthaceae. The ovule is hemi-orthotropous and pendant with endotestal-endotegmic organization and distinct crystalliferous endotesta similar to that in *Canrightia* and Chloranthaceae. Unlike *Canrightia* the new taxon apparently lacks endothelium cells, but has a well-developed tegmen, both features that are also seen in Chloranthaceae. However, unlike extant Chloranthaceae the fossil shows scars from several, separate stamens on each fruit. A further observation made possible by SRXTM is that seeds enclosed in the fruit wall have an endotesta with a distinctive pitted outer surface. Based on this information it has been possible to link the fruits with dispersed, pitted seeds that occur abundantly in some of the mesofossil floras.

Scandianthus, Silvianthemum, *and* Bertilanthus*: Late Cretaceous asterid flowers with strong Gondwanan relationships*.—Flowers of *Scandianthus* Friis and Skarby 1982 from the Late Cretaceous Åsen locality were the first fossil flowers to be formally described from Cretaceous mesofossil assemblages (Friis and Skarby, 1982). They are known from a series of ontogenetic stages that range from flower buds (Figs. 7, 8.1–8.3) to mature fruits (Fig. 8.4–8.9). Specimens also show variation in preservation from fossils that are strongly charcoalified to lignitized fossils. One specimen is particularly interesting in having two tiny buds, only about 0.5 mm in diameter, preserved in a very early developmental stage (Fig. 7). In the original description of the genus two species were established. Based on serial sectioning and SEM of fragmentary specimens the placentation was interpreted as apical and pendant. The presence of apical and pendant placentae is now confirmed by SRXTM analyses of specimens in different developmental stages. In the very young floral buds the placentae are seen as small protrusions (Fig. 7.4, 7.6) and in more mature specimens the apical placentae have numerous small ovules (Fig. 8.4, 8.6, 8.9). Sepals are persistent (Fig. 8.4–8.8), while petals are only preserved in the buds (Figs. 7.5, 8.1, 8.2). In pre-anthetic flowers petals are abscised (Fig. 8.4–8.8). Comparison with extant taxa showed close relationship to extant flowers previously included in the Saxifragaceae (Engler, 1930) or Saxifragales (Takhtajan, 1969). In particular, flowers of *Scandianthus* showed close similarity to those of extant *Vahlia* Thunb. that have similar pendant placentation (Friis and Skarby, 1982).

Vahlia is a Gondwanan taxon restricted to South Africa and is now included in its own family (Vahliaceae). The systematic position of the genus is still not fully resolved, but based on molecular phylogenetics the family is placed in the asterid clade close to the lamiids in the APGIII (2009) classification, and is perhaps sister to the Boraginaceae. If this relationship between *Scandianthus* and *Vahlia* is correct the lineage that includes extant *Vahlia* may have once been present in the Northern Hemisphere. To test this hypothesis a reinvestigation of *Scandianthus* using SRXTM and in depth comparison with extant *Vahlia* has now been initiated in the same way as comparison between *Silvianthemum*/*Bertilanthus* and *Quintinia* (see below). Preliminary investigations show exquisite details also including the organization of perianth and androecium as well as details of the placenta that are important for a more detailed comparison with extant *Vahlia*.

Silvianthemum Friis (1990) and *Bertilanthus* Friis and Pedersen (2012) are two other fossil taxa based on well-preserved fossil flowers from the Late Cretaceous Åsen locality (Friis, 1990; Friis and Pedersen, 2012). Like *Scandianthus*, *Silvianthemum* was originally compared to a Gondwanan member of the Saxifragaceae/Saxifragles (extant *Quintinia*) that is now resolved as a member of the asterid clade based on molecular phylogenetics. Most specimens of *Silvianthemum* and *Bertilanthus* are preserved in the post-anthetic state as open flowers or mature fruits, and petals and stamens are usually lost. However, SRXTM of rare flowers buds, including the holotype of *Silvianthemum* (Figs. 2, 9.6) has revealed important information on floral organization. In particular, the unusual number of stamens (eight) in the pentamerous flowers of *Silvianthemum* has now been documented securely by SRXTM.

The original systematic placement of *Silvianthemum* was suggested based mainly on a review of the relevant literature. However, the application of SRXTM to the fossil flowers now allows more detailed comparison with extant *Quintinia* and confirms the close relationship among the three genera (Friis et

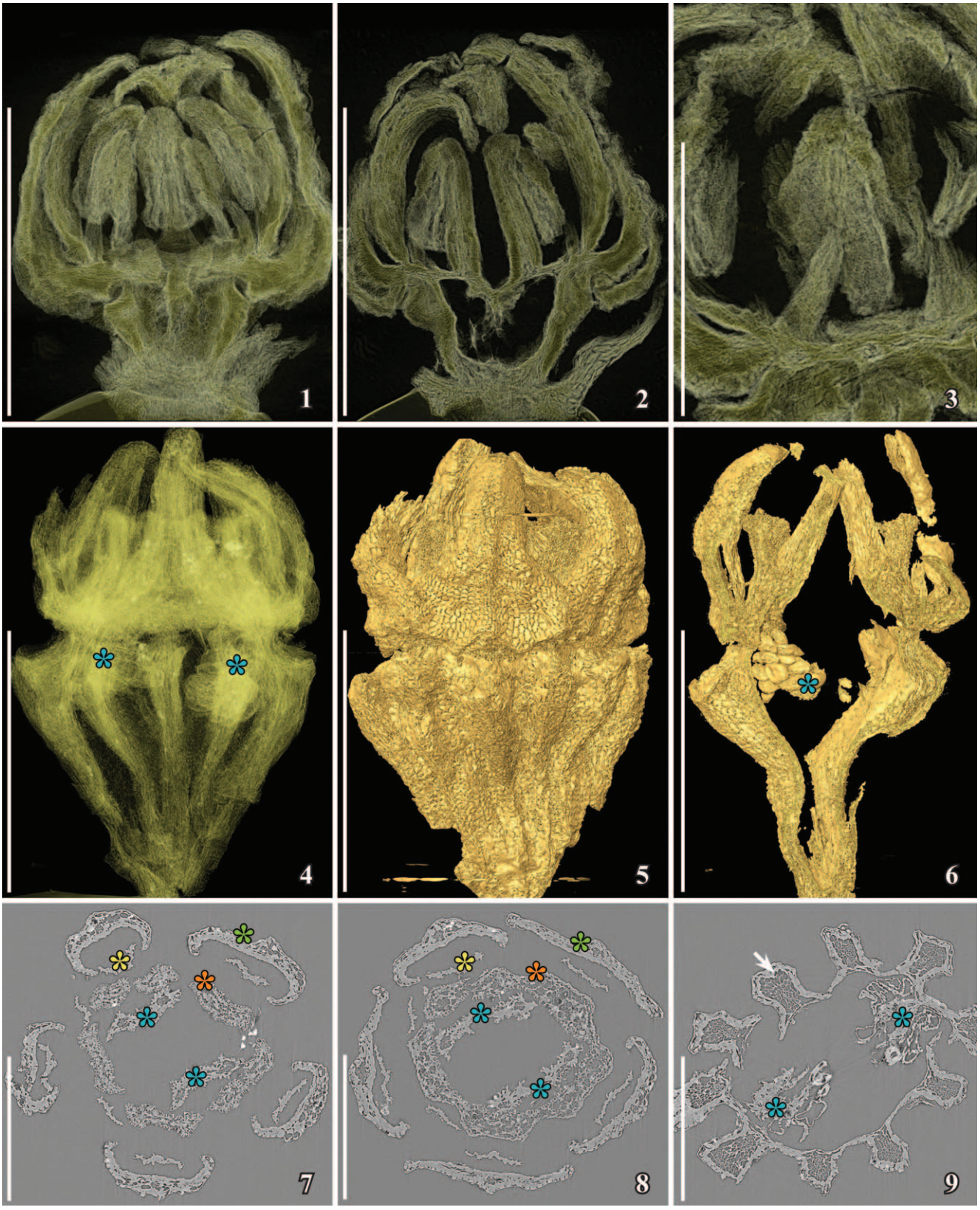

Figure *8*—SRXTM reconstructions of *Scandianthus costatus* from the Late Cretaceous Åsen locality, Sweden; *1–3*, 3-D cut longitudinal voltex reconstructions (transparent renderings) of small lignitized flower bud (S172368) showing inferior ovary and sepals and petals covering androecium and styles (*1*, *2*), inner whorl of stamens closely adpressed to the two free styles (*2*), and stamens with short filaments and sagittate, dorsifixed anthers (*1–3*); section in *1* between orthoslices yz875 and 1075, section in *2* between orthoslices yz770–870 and section in *3* between yz440–560; dataset acquired using 10× objective and a 20 µm thick LAG:Ce scintillator at 10 keV (voxel size 0.74 µm); *4–9*, reconstructions of mature, charcoalified specimens (S174119) with strongly ribbed inferior ovary and persistent calyx; dataset acquired using 10× objective and a 20 µm thick LAG:Ce scintillator at 10 keV (voxel size 0.65 µm); *4–6*, 3-D reconstructions of flower in cut longitudinal voltex (transparent rendering) (*4*) and cut isosurface rendering (*5*, *6*), showing persistent sepals (*4*, *5*), stamens with extended filaments, but

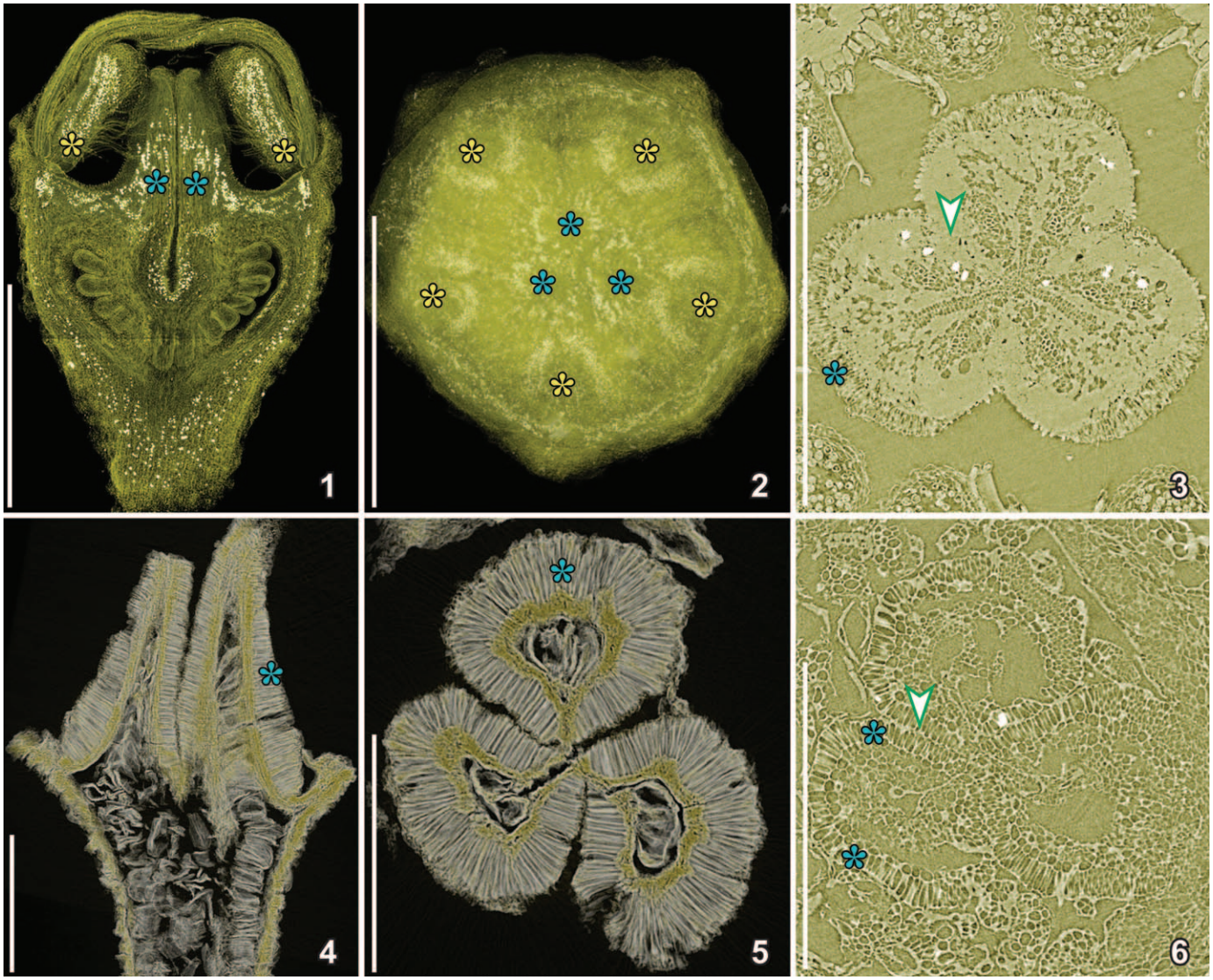

Figure 9—*1–3*, SRXTM reconstructions of a flower of extant *Quintinia quatrefagesii* from North Queensland, Australia, dataset acquired using 10× objective and a 20 μm thick LAG:Ce scintillator at 10 keV (voxel size 0.74 μm) with vertical stacking; specimen critically point dried prior to SRXTM; *1*, 3-D cut voltex (transparent rendering) reconstruction of flower bud in lateral view showing internal details of flower and densely-spaced crystals, seen as whitish flecks, particularly in the anthers (yellow asterisks) and carpels (blue asterisks); *2*, 3-D voltex (transparent rendering) reconstruction of flower bud in apical view showing the pentamerous organization with the five stamens (yellow asterisks) and three styles (blue asterisks) demarcated by concentrations of crystals; *3*, 2-D transverse orthoslice in the region of the styles with dorsal palisade cells (blue asterisk) of the styles and postgenital fusion of the carpels (arrowhead); *4–6*, SRXTM reconstructions of *Silvianthemum suecicum* from the Late Cretaceous Åsen locality, Sweden; *4*, *5*, 3-D cut voltex (transparent rendering) reconstruction of post-anthetic flower (S171578) in longitudinal (*4*) and transverse (*5*) orientations showing prominent palisade cells of the styles (blue asterisks) and placentation that extends into the apocarpous region of the carpels; dataset acquired using 10× objective and a 20 μm thick LAG:Ce scintillator at 10 keV (voxel size 0.74 μm); *6*, 2-D transverse orthoslice of a flower bud (holotype of *Silvianthemum suecicum*) through the three styles, showing palisade cells (blue asterisk) of styles extending from ventral to dorsal side and postgenital fusion of carpels (arrowhead) (same dataset as for Fig. *2*). Scale bars for *1*, *2*, *4*, *5*=500 μm; for *3*, *6*=250 μm.

al., 2013b). *Quintinia* has short sepals and free, quincuncial petals (Fig. 9.1, 9.2), as is seen also in *Silvianthemum* and *Bertilanthus*. An especially distinctive feature that links fossil *Silvianthemum* and *Bertilanthus* with extant *Quintinia* is the presence of distinct palisade cells in the styles. In *Silvianthemum* and *Bertilanthus* the palisade cells are more pronounced than in *Quintinia* and these occur both on the ventral and dorsal sides (Fig. 9.4–9.6). In *Quintinia* they are restricted to the dorsal side of the styles (Fig. 9.3). These and other critical features strongly reinforce the close relationships of the three genera (Friis et al., 2013b). The current distribution of *Quintinia* is from Australia, New Zealand, Vanuatu, New Caledonia, New Guinea, and the Philippines.

←
abscised anthers (*4*, *6*), apical placentae with small ovules/seeds (*4*, *6*, blue asterisk) and ovary open between the styles (*6*), *7*, *8*, 2-D transverse orthoslices through flower showing sections through middle (*7*) and basal (8) part of perianth with whorl of five sepals (one marked with green asterisk), petals are abscised, the flattened filaments (one marked with yellow asterisk) of two whorls of five stamens of which three inner stamens are abscised, five-lobed nectary (one lobed marked with orange asterisk) and the two split styles (blue asterisk); *9*, section at the level of the placentae showing the pronounced ribs (one rib marked with arrow) of the ovary wall with well-preserved vascular bundles of narrow cells, hanging placentae (blue asterisk) and tiny ovules/seeds. Scale bars for *1*, *2*, *7–9*=500 μm; for *3*=250 μm; for *4–6*=1 mm.

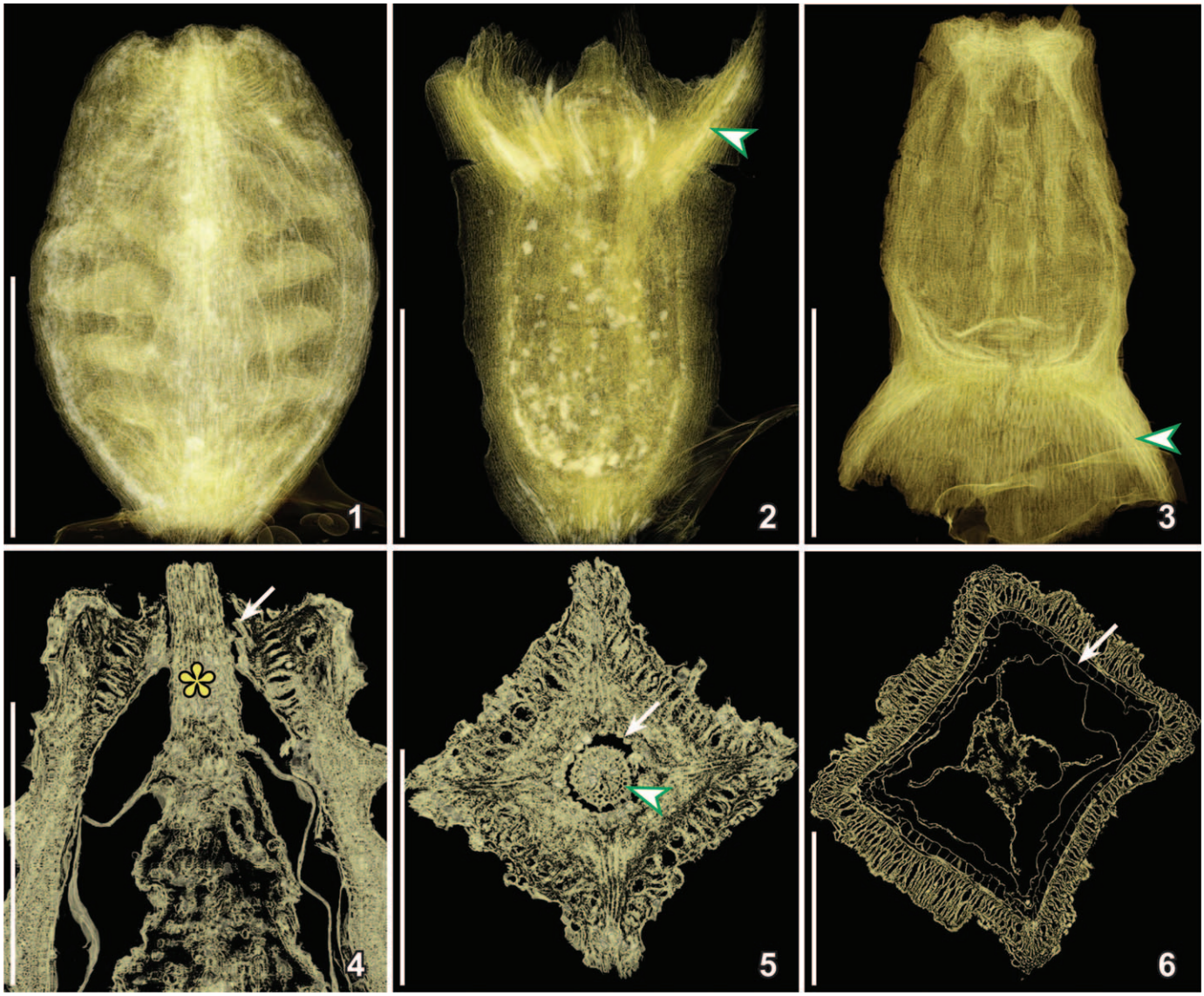

Figure *10*—SRXTM reconstructions of chlamydospermous seeds from the Early Cretaceous of North America (*1*, *3*, *4–6*) and Portugal (*2*). *1*, 3-D voltex (transparent rendering) reconstruction of seed of *Acanthocatia virginiensis* Friis, Pedersen and Crane, 2013a (PP53723), from the Puddledock locality in lateral view showing the rugulate surface and the shape of the sclerenchyma cells; dataset acquired using 20× objective and a 20 μm thick LAG:Ce scintillator at 10 keV (voxel size 0.37 μm); *2*, 3-D voltex (transparent rendering) reconstruction of seed of *Tomcatia taylorii* Friis, Pedersen and Crane, 2013a (S154562), from the Torres Vedras locality, in lateral view showing the distinct apical projections (arrowhead) formed from tubular cells that are partly filled by crystals, seen as lighter flecks; dataset acquired using 20× objective and a 20 μm thick LAG:Ce scintillator at 10 keV (voxel size 0.37 μm); *3*, 3-D voltex (transparent rendering) reconstruction of seed of *Cattomia trapezoides* Friis, Pedersen and Crane, 2013a (PP53720), from the Puddledock locality in lateral view showing the distinct basal skirt (arrowhead) comprised of tubular cells; dataset acquired using 10× objective and a 20 μm thick LAG:Ce scintillator at 10 keV (voxel size 0.74 μm); *4–6*, 3-D cut voltex (transparent rendering) reconstruction of *Acanthocatia virginiensis* (same dataset as for *1*); *4*, longitudinal section through the apical part of the seed showing thick outer seed envelope of sclerenchyma cells enclosing the membranous integument that extends apically into long micropylar tube (yellow asterisk) and papillate lining of sclerenchyma in the micropylar region (arrow); *5*, transverse section through the seed in micropylar region showing the micropylar canal closed by radiating cells of inner epidermis of integument (arrowhead) and papillate lining of the sclerenchyma layer (arrow); *6*, transverse section through the middle of seed showing the thick sclerenchyma layer of the seed envelope with thin-walled inner epidermal cell (arrow) surrounding the thin tissues of integument and nucellus. Scale bars for *1–3*=500 μm; for *4–6*=250 μm.

The close relationship to the two Late Cretaceous taxa from Åsen suggests a much wider distribution of the group in earlier geological periods. If a similar pattern can also be substantiated for a group including fossil *Scandianthus* and extant *Vahlia* this will open up interesting new aspects in the study of angiosperm biogeography.

Tomcatia *and the Early Cretaceous chlamydosperm complex*.—The application of SRXTM has been instrumental in the recognition of a diverse complex of seeds with a chlamydospermous seed organization in Early Cretaceous mesofossil floras (Fig. 10). In general organization these seeds are very similar to seeds of Erdtmanithecales and Gnetales. The nucellus is enclosed by both a thin membraneous integument and a thick sclerenchymatic seed envelope (Fig. 10.4–10.6). The integument is extended into a long slender micropylar tube (Fig. 10.4) that in mature seeds is typically closed by extension of the inner epidermal cells towards the center of the micropylar canal (Fig. 10.5). Similar seed organization has also been observed for seeds of Bennettitales and based on these distinctive features of

seed organization we have suggested close relationship between the Bennettitales, Erdtmanithecales and Gnetales (Pedersen et al., 1989; Friis et al., 2007; Mendes et al., 2008; Friis et al., 2009a, 2013a; but see also Rothwell et al., 2009 for alternative interpretation).

The most peculiar of the Early Cretaceous chlamydospermous seeds are those referred to *Tomcatia*, which are unusual in having four elongated, distal projections, one on each corner of the seed (Fig. 10.2). These structures were first interpreted as possible tepals of a tetramerous flower (Friis et al., 1994), but SRXTM studies revealed a distinctly chlamydospermous seed organization (Friis et al., 2007). The SRXTM screening of numerous other fossil seeds of potential similar organization has recognized more than 30 different species from the Early Cretaceous of Portugal and North America that are broadly assignable to this complex. Seventeen species in 11 genera have been described so far (*Acanthocatia* Friis et al., 2013a; *Buarcospermum* Friis et al., 2009; *Cattomia* Friis et al., 2013a; *Ephedrispermum* Rydin et al., 2006; *Erdtmanispermum* Pedersen et al., 1989; *Lignierispermum* Friis et al., 2009; *Lobospermum* Friis et al., 2009; *Quadrispermum* Friis et al., 2013a; *Raunsgaardispermum* Mendes et al., 2008; *Rugonella* Friis et al., 2009; and *Tomcatia* Friis et al., 2013a, and the formal description of several other taxa is underway (e.g., Friis et al. 2014a). Other Early Cretaceous seeds with very similar construction have also been assigned to the extant genus *Ephedra* L. (Rydin et al., 2006).

Critical features of many of these seeds would have been very difficult to discern without SRXTM. For example, both the integument and the tubular micropylar extension of the integument are delicate, membranous, and often not well preserved. With SRXTM features of the integument in the micropylar area including closure of the micropylar canal by radial expansions of the cells of the inner epidermis can be examined in detail allowing comparison between the various mesofossils as well as other extant and extinct taxa. SRXTM also revealed that the projections in *Tomcatia* were mainly composed of distinctive tubular cells (Fig. 10.2). The same kind of tubular cells were observed in *Cattomia* where they are particularly well developed at the base of the seed (Fig. 10.3). Similar tubular cells have also been described from seeds of Bennettitales (Friis et al., 2013a).

CONCLUSIONS

The number of potential applications of SRXTM in paleobiology is vast. SRXTM has already been informative where it has been deployed in paleobotany, but the full possibilities of these techniques are still relatively underexplored. The examples provided above illustrate the diverse situations in which the use of SRXTM data and its visualization has provided new and critical information on internal structure. Furthermore, while we have shown here only examples where SRXTM has been applied to charcoalified and lignitized specimens, excellent results have also been obtained with other kinds of material. These include permineralized bennettitalean ovulate structures, various organs of ferns and angiosperm fruits that are currently under investigation. This kind of material requires higher energies, and particularly for larger specimens where lateral merging and vertical stacking is required the acquisition time may be extensive.

Disappointingly, experiments with strongly compressed specimens with homogenized coalified tissue from Jurassic sediments have failed to provide details of cells and tissues. New methods of pre-preparation will need to be devised if such specimens are to yield useful information with SRXTM. Nevertheless, the capability of SRXTM studies to provide details of internal structure in a new way from a great range of fossil material significantly extends the structural and anatomical information that can potentially be obtained from fossil plants. In many cases with coalified mesofossil material the level of detail that can be obtained rivals, or exceeds, that can be obtained from the conventional study of permineralizations. The combination of SRXTM with the availability of a large numbers of diverse and well-preserved specimens offers the possibility of a new phase of rapid progress in our understanding of Cretaceous and other fossil plants.

Field work and sample preparation will continue to be the necessary foundation searching for new fossil material, but the introduction of SRXTM will also result in a significant change in the nature of research protocols being deployed. In particular, it largely shifts the efforts of the investigator from preparation work in the laboratory to analysis and visualization on the computer. This shift is emblematic of a broader trend, manifested in many areas of science, toward the rapid acquisition of very large data sets that require significant computer capability to be processed and used to their maximum extent.

In many cases, the critical details revealed by the application of SRXTM have created opportunities to compare the fine structure of fossils with those of extant taxa, raising the possibility of also using SRXTM to study complex 3-D structures in living plants. While conventional sectioning will probably continue to be the most convenient technique for investigating the internal structure of extant plants SRXTM is likely to prove particularly valuable in some cases, for example, where combinations of especially hard, delicate or crystal filled tissues make conventional sectioning difficult.

While SRXTM has already proved valuable for interpretation of critical internal details in a range of fossils there is considerable potential for further technical refinements that will make possible new levels of analysis. For example, the coupling of higher magnification microscope objectives with thinner scintillators could push the spatial resolution to the submicron regime. Ultimately this may allow investigation of pollen in situ in the fossil flowers, megaspore membranes in seeds, cuticle microstructures, and many other microscopic features that currently require conventional preparation for light or electron microscopy. These and other advances will ensure that SRXTM will inevitably become a widely used tool for the detailed study of fossil plants of all kinds.

ACKNOWLEDGMENTS

We thank S. Bengtson, A. Lindström, V. Belivanova, and T. Hultgren for help with the SRXTM analyses. We also thank two anonymous reviewers for helpful comments to the manuscript. This work was supported by the Swedish Natural Science Research Council (EMF). SRXTM was funded by the SLS (European Union FP6 project 20100167 as well as several previous projects to P. C. J. Donoghue, S. Bengtson, and E. M. Friis).

REFERENCES

APGIII. 2009. An update of the Angiosperm Phylogeny Group classification for the orders and families of flowering plants: APG III. Botanical Journal of the Linnean Society, 161:105–121.

Boas, F. E. and D. Fleischmann. 2011. Evaluation of two iterative techniques for reducing metal artifacts in computed tomography. Radiology, 259:894–902.

Boin, M. and A. Haibel. 2006. Compensation of ring artefacts in synchrotron tomographic imaging. Optics Express, 14:12071–12075.

Bonse, U. and M. Hart. 1965. An X-ray interferometer with long separated interfering beam paths (E). Applied Physics Letters, 7:99–100.

BRONNIKOV, A. V. 2002. Theory of quantitative phase-contrast computed tomography. Journal of the Optical Society of America A, 19:472–480.

BROWN, S. A. E., A. C. SCOTT, I. J. GLASSPOOL, AND M. E. COLLINSON. 2012. Cretaceous wildfires and their impact on the Earth system. Cretaceous Research, 36:162–190.

CHANDLER, M. E. J. 1957. The Oligocene flora of the Bovey Tracey Lake Basin (Devonshire). Bulletin of the British Museum (Natural History) Geology, 3:7–123.

CHAPMAN, D., W. THOMLINSON, R. E. JOHNSTON, D. WASHBURN, E. PISANO, N. GMUR, Z. ZHONG, R. MENK, F. ARFELLI, AND D. SAYERS. 1997. Diffraction enhanced x-ray imaging. Physics in Medicine and Biology, 42:2015–2025.

CLOETENS, P., R. BARRETT, J. BARUCHEL, J. P. GUIGAY, AND M. SCHLENKER. 1996. Phase objects in synchrotron radiation hard x-ray imaging. Journal of Physics D-Applied Physics, 29:133–146.

CLOETENS, P., W. LUDWIG, J. BARUCHEL, D. VAN DYCK, J. VAN LANDUYT, J. P. GUIGAY, AND M. SCHLENKER. 1999. Holotomography: quantitative phase tomography with micrometer resolution using hard synchrotron radiation x rays. Applied Physics Letters, 75:2912–2914.

COLLINSON, M. E., S. R. MANCHESTER, AND V. WILDE. 2013a. Fossil fruits and seeds of the middle Eocene Messel biota, Germany. Abhandlungen der Senckenberg Gesellschaft für Naturforschung, 570:1–251.

COLLINSON, M. E., S. Y. SMITH, J. H. A. VAN KONIJENBURG-VAN CITTERT, D. J. BATTEN, J. VAN DER BURGH, J. BARKE, AND F. MARONE. 2013b. New observations and synthesis of Paleogene heterosporous water ferns. International Journal of Plant Sciences, 174:350–363.

CRANE, P. R. AND P. S. HERENDEEN. 2009. Bennettitales from the Gristhorpe Bed (Middle Jurassic) at Cayton Bay, Yorkshire, U.K. American Journal of Botany, 96:284–295.

DAVIS, T. J., D. GAO, T. E. GUREYEV, A. W. STEVENSON, AND S. W. WILKENS. 1995. Phase-contrast imaging of weakly absorbing materials using hard X-rays. Nature, 373:595–598.

DOROFEEV, P. I. 1963. Treticnye flory Zapadnoj Sibiri. Izd. Akad. nauk SSSR, Moscow and Leningrad, p. 1–345.

DRINNAN, A. N., P. R. CRANE, E. M. FRIIS, AND K. R. PEDERSEN. 1990. Lauraceous flowers from the Potomac Group (mid-Cretaceous) of eastern North America. Botanical Gazette, 151:370–384.

EDWARDS, D. 1996. New insights into early land ecosystems: A glimpse of a lilliputian world. Review of Palaeobotany and Palynology, 90:159–174.

ENGLER, A. 1930. Saxifragaceae, p. 74–226. *In* A. Engler and H. Prantl, Die natürlichen Pflanzenfamilien, Bd. 18. Engelmann, Leipzig.

ERIKSSON, O., E. M. FRIIS, AND P. LÖFGREN. 2000a. Seed size, fruit size and dispersal spectra in angiosperms from the Early Cretaceous to the late Tertiary. American Naturalist, 156:47–58.

ERIKSSON, O., E. M. FRIIS, K. R. PEDERSEN, AND P. R. CRANE. 2000b. Seed size and dispersal systems of Early Cretaceous angiosperms from Famalicão, Portugal. International Journal of Plant Sciences, 161:319–329.

FRIIS, E. M. 1985. Angiosperm fruits and seeds from the middle Miocene of Jutland (Denmark). Biologiske Skrifter, Det Kongelige Danske Videnskabernes Selskab, 24:1–165.

FRIIS, E. M. 1990. *Silvianthemum suecicum* gen. et sp. nov., a new saxifragalean flower from the Late Cretaceous of Sweden. Biologiske Skrifter, Det Kongelige Danske Videnskabernes Selskab, 36:1–35.

FRIIS, E. M., P. R. CRANE, AND K. R. PEDERSEN. 2011. Early flowers and angiosperm evolution. Cambridge University Press, Cambridge, p. 1–585.

FRIIS, E. M., P. R. CRANE, K. R. PEDERSEN, S. BENGTSON, P. C. J. DONOGHUE, G. W. GRIMM, AND M. STAMPANONI. 2007. Phase contrast enhanced synchrotron-radiation X-ray analyses of Cretaceous seeds link Gnetales to extinct Bennettitales. Nature, 450:549–552.

FRIIS, E. M. AND K. R. PEDERSEN. 2011. *Canrightia resinifera* gen. et sp. nov., a new extinct angiosperm with *Retimonocolpites*-type pollen from the Early Cretaceous of Portugal: Missing link in the eumagnoliid tree? Grana, 50:3–29.

FRIIS, E. M. AND K. R. PEDERSEN. 2012. *Bertilanthus scanicus*, a new asterid flower from the Late Cretaceous (late Santonian–early Campanian) of Scania, Sweden. International Journal of Plant Sciences, 173:318–330.

FRIIS, E. M., K. R. PEDERSEN, AND P. R. CRANE. 1992. *Esgueiria* gen. nov., fossil flowers with combretaceous features from the Late Cretaceous of Portugal. Biologiske Skrifter, Det Kongelige Danske Videnskabernes Selskab, 41:1–45.

FRIIS, E. M., K. R. PEDERSEN, AND P. R. CRANE. 1994. Angiosperm floral structures from the Early Cretaceous of Portugal. Plant Systematics and Evolution, 8:31–49.

FRIIS, E. M., K. R. PEDERSEN, AND P. R. CRANE. 1999. Early angiosperm diversification: the diversity of pollen associated with angiosperm reproductive structures in Early Cretaceous floras from Portugal. Annals of the Missouri Botanical Garden, 86:259–296.

FRIIS, E. M., K. R. PEDERSEN, AND P. R. CRANE. 2000. Reproductive structure and organization of basal angiosperms from the Early Cretaceous (Barremian or Aptian) of Western Portugal. International Journal of Plant Sciences, 161:S169–S182.

FRIIS, E. M., K. R. PEDERSEN, AND P. R. CRANE. 2001. Fossil evidence of water lilies (Nymphaeales) in the Early Cretaceous. Nature, 410:357–360.

FRIIS, E. M., K. R. PEDERSEN, AND P. R. CRANE. 2009a. Early Cretaceous mesofossils from Portugal and eastern North America related to the Bennettitales-Erdtmanithecales-Gnetales group. American Journal of Botany, 96:252–283.

FRIIS, E. M., K. R. PEDERSEN, AND P. R. CRANE. 2010. Cretaceous diversification of angiosperms in the western part of the Iberian Peninsula. Review of Palaeobotany and Palynology, 162:341–361.

FRIIS, E. M., K. R. PEDERSEN, AND P. R. CRANE. 2013a. New diversity among chlamydospermous seeds from the Early Cretaceous of Portugal and North America. International Journal of Plant Sciences, 173:530–558.

FRIIS, E. M., K. R. PEDERSEN, AND P. R. CRANE. 2014a. Welwitschioid diversity in the Early Cretaceous: Evidence from fossil seeds with pollen from Portugal and eastern North America. Grana, in press.

FRIIS, E. M., K. R. PEDERSEN, AND P. K. ENDRESS. 2013b. Floral structure of extant *Quintinia* (Paracryphiales, Campanulids) compared with the Late Cretaceous *Silvianthemum* and *Bertilanthus*. International Journal of Plant Sciences, 174:647–664.

FRIIS, E. M., K. R. PEDERSEN, AND F. MARONE. 2014b. *Arcellites punctatus* sp. nov.: A new megaspore from the Early Cretaceous of Portugal studied using high resolution synchrotron radiation x-ray tomographic microscopy (SRXTM). Grana, in press.

FRIIS, E. M., K. R. PEDERSEN, AND J. SCHÖNENBERGER. 2003. *Endressianthus*, a new Normapolles producing plant genus of fagalean affinity from the Late Cretaceous of Portugal. International Journal of Plant Sciences, 164 (5 Suppl.):S201–S223.

FRIIS, E. M., K. R. PEDERSEN, M. VON BALTHAZAR, G. W. GRIMM, AND P. R. CRANE. 2009b. *Monetianthus mirus* gen. et sp. nov., a nymphaealean flowers from the Early Cretaceous of Portugal. International Journal of Plant Sciences, 170:1086–1101.

FRIIS, E. M. AND A. SKARBY. 1981. Structurally preserved angiosperm flowers from the Upper Cretaceous of southern Sweden. Nature, 291:485–486.

FRIIS, E. M. AND A. SKARBY. 1982. *Scandianthus* gen. nov., angiosperm flowers of saxifragalean affinity from the Upper Cretaceous of southern Sweden. Annals of Botany, 50:569–583.

GANDOLFO, M. A., K. C. NIXON, AND W. L. CREPET. 2004. Cretaceous flowers of Nymphaeaceae and implications for complex insect entrapment pollination mechanisms in early angiosperms. Proceedings of the National Academy of Sciences, U.S.A., 101:8056–8060.

GROSO, A., R. ABELA, AND M. STAMPANONI. 2006. Implementation of a fast method for high resolution phase contrast tomography. Optics Express, 14: 8103–8110.

HABERTHÜR, D., C. HINTERMÜLLER, F. MARONE, J. C. SCHITTNY, AND M. STAMPANONI. 2010. Radiation dose optimized lateral expansion of the field of view in synchrotron radiation X-ray tomographic microscopy. Journal of Synchrotron Radiation, 17:590–599.

HARRIS, T. M. 1981. Burnt ferns from the English Wealden. Proceedings of the Geologists' Association, 92:47–58.

HEŘMANOVÁ, Z., J. KVAČEK, AND E. M. FRIIS. 2011. *Budvaricarpus serialis* Knobloch and Mai, an unusual new member of the Normapolles complex from the Late Cretaceous of the Czech Republic. International Journal of Plant Sciences, 172:285–293.

KAK, A. C. AND M. SLANEY. 2001. Principles of computerized tomographic imaging. Society of Industrial and Applied Mathematics, Philadelphia, PA, p. 1–327.

KIRCHHEIMER, F. 1957. Die Laubgewächse der Braunkohlenzeit. Wilhelm Knapp Verlag, Halle, p. 1–783.

LUPIA, R. 1995. Paleobotanical data from fossil charcoal: an actualistic study of seed plant reproductive structures. Palaios, 10:465–477.

MADER, K., F. MARONE, C. HINTERMÜLLER, G. MIKULJAN, A. ISENEGGER, AND M. STAMPANONI. 2011. High-throughput full-automatic synchrotron-based tomographic microscopy. Synchrotron Radiation, 18:117–124.

MAI, D. H. 1995. Tertiäre Vegetationsgeschichte Europas. Gustav Fischer Verlag, Jena, Stuttgart, New York, p. 1–691.

MARONE, F., B. MÜNCH, AND M. STAMPANONI. 2010. Fast reconstruction algorithm dealing with tomography artifacts. *In* S. R. Stock, Developments in X-Ray Tomography Vii, San Diego, Proceedings of SPIE-The International Society for Optical Engineering.

MARONE, F. AND M. STAMPANONI. 2012. Regridding reconstruction algorithm for real-time tomographic imaging. Journal of Synchrotron Radiation, 19: 1029–1037.

MENDES, M. M., J. DINIS, J. PAIS, AND E. M. FRIIS. 2014. Vegetational composition of the Early Cretaceous Chicalhão flora (Lusitanian Basin, western Portugal) based on palynological and mesofossil assemblages. Review of Palaeobotany and Palynology, 200:65–81.

MENDES, M. M., J. PAIS, AND E. M. FRIIS. 2008. *Raunsgaardispermum lusitanicum* gen. et sp. nov., a new seed with *in situ* pollen from the Early Cretaceous (probably Berriasian) of Portugal: Further support for the Bennettitales-Erdtmanithecales-Gnetales link. Grana, 47:211–219.

MOHR, B. A. R., M. E. C. BERNARDES-DE-OLIVEIRA, AND D. W. TAYLOR. 2008. *Pluricarpellatia*, a nymphaealean angiosperm from the Lower Cretaceous of northern Gondwana (Crato Formation, Brazil). Taxon, 57:1147–1158.

MOREAU, J.-D., P. CLOETENS, B. GOMEZ, V. DAVIERO-GOMEZ, D. NÉRAUDEAU, T. A. LAFFORD, AND P. TAFFOREAU. 2014. Multiscale 3D virtual dissections of 100-million-year-old flowers using X-Ray synchrotron micro and nano-tomography. Microscopy and Microanalysis, 20:305–312.

MÜNCH, B., P. TRTIK, F. MARONE, AND M. STAMPANONI. 2009. Stripe and ring artifact removal with combined wavelet-Fourier filtering. Optics Express, 17:8567–8591.

PAGANIN, D., S. C. MAYO, T. E. GUREYEV, P. R. MILLER, AND S. W. WILKINS. 2002. Simultaneous phase and amplitude extraction from a single defocused image of a homogeneous object. Journal of Microscopy-Oxford, 206:33–40.

PEDERSEN, K. R., P. R. CRANE, AND E. M. FRIIS. 1989. Pollen organs and seeds with *Eucommiidites* pollen. Grana, 28:279–294.

PRELL, D., Y. KYRIAKOU, M. KACHELRIESS, AND W. A. KALENDER. 2010. Reducing metal artifacts in computed tomography caused by hip endoprostheses using a physics-based approach. Investigative Radiology, 45:747–754.

RASHID-FARROKHI, F., K. J. R. LIU, C. A. BERENSTEIN, AND D. WALNUT. 1997. Wavelet-based multiresolution local tomography. Transactions on Image Processing, 6:1412–1430.

REID, C. AND E. M. REID. 1915. The Pliocene floras of the Dutch Prussian border. Mededelingen van de Rijksopsporing van Delfstoffen, 6:1–178.

ROTHWELL, G. W., W. L. CREPET, AND R. A. STOCKEY. 2009. Is the anthophyte hypothesis alive and well? New evidence from the reproductive structures of Bennettitales. American Journal of Botany, 96:296–322.

RYDIN, C., K. R. PEDERSEN, P. R. CRANE, AND E. M. FRIIS. 2006. Former diversity of *Ephedra* (Gnetales): evidence from Early Cretaceous seeds from Portugal and North America. Annals of Botany, 98:123–140.

SCHÖNENBERGER, J. AND E. M. FRIIS. 2001. Fossil flowers of ericalean s.l. affinity from the Late Cretaceous of southern Sweden. American Journal of Botany, 88:467–480.

SCHÖNENBERGER, J., E. M. FRIIS, M. L. MATTHEWS, AND P. K. ENDRESS. 2001a. Cunoniaceae in the Cretaceous of Europe: evidence from fossil flowers. Annals of Botany, 88:423–437.

SCHÖNENBERGER, J., K. R. PEDERSEN, AND E. M. FRIIS. 2001b. Normapolles flowers of fagalean affinity from the Late Cretaceous of Portugal. Plant Systematics and Evolution, 226:205–230.

SCHÖNENBERGER, J., M. VON BALTHAZAR, M. TAKAHASHI, X. XIAO, P. R. CRANE, AND P. S. HERENDEEN. 2012. *Glandulocalyx upatoiensis*, a fossil flower of Ericales (Actinidiaceae/Clethraceae) from the Late Cretaceous (Santonian) of Georgia, U.S.A. Annals of Botany, 109:921–936.

SCOTT, A. C., J. GALTIER, N. J. GOSTLING, S. Y. SMITH, M. E. COLLINSON, M. STAMPANONI, F. MARONE, P. C. J. DONOGHUE, AND S. BENGTSON. 2009. Scanning electron microscopy and synchrotron radiation X-ray tomographic microscopy of 330 million year old charcoalified seed fern fertile organs. Microscopy and Microanalysis, 15:166–173.

SCOTT, A. C. AND T. P. JONES. 1991. Microscopical observations of recent and fossil charcoal. Microscopy and Analysis, July 1991:13–15.

SIJBERS, J. AND A. POSTNOVZ. 2004. Reduction of ring artefacts in high resolution micro-CT reconstructions. Physics in Medicine and Biology, 49: N247–N253.

SLATER, B. J., S. MCLOUGHLIN, AND J. HILTON. 2011. Guadalupian (Middle Permian) megaspores from a permineralised peat in the Bainmedart Coal Measures, Prince Charles Mountains, Antarctica. Review of Palaeobotany and Palynology, 167:140–155.

SMITH, S. Y., M. E. COLLINSON, P. J. RUDALL, D. A. SIMPSON, F. MARONE, AND M. STAMPANONI. 2009a. Virtual taphonomy using synchrotron tomographic microscopy reveals cryptic features and internal structure of modern and fossil plants. Proceedings of the National Academy of Sciences, 106: 12013–12018.

SMITH, S. Y., M. E. COLLINSON, D. A. SIMPSON, P. J. RUDALL, F. MARONE, AND M. STAMPANONI. 2009b. Elucidating the affinities and habitat of ancient, widespread Cyperaceae: *Volkeria messelensis* gen. et sp. nov., a fossil mapanioid sedge from the Eocene of Europe. American Journal of Botany, 96:1506–1518.

SNIGIREV, A., I. SNIGIREVA, V. KOHN, S. KUZNETSOV, AND I. SCHELOKOV. 1995. On the possibilities of x-ray phase contrast microimaging by coherent high-energy synchrotron radiation. Review of Scientific Instruments, 66:5486–5492.

STAEDLER, Y. M., D. MASSON, AND J. SCHÖNENBERGER. 1913. Plant tissues in 3D via X-ray tomography: Simple contrasting methods allow high resolution imaging. PlosOne, 8:1–10.

STAMPANONI, M., A. GROSO, A. ISENEGGER, G. MIKULJAN, Q. CHEN, A. BERTRAND, S. HENEIN, R. BETEMPS, U. FROMMHERZ, P. BOHLER, D. MEISTER, M. LANGE, AND R. ABELA. 2006. Trends in synchrotron-based tomographic imaging: the SLS experience, p. 780410-1/11. *In* U. Bonse, Developments in X-Ray Tomography V, Proceedings of the Society of Photo-Optical Instrumentation Engineers (SPIE).

TAKHTAJAN, A. L. 1969. Flowering plants. Origin and dispersal. Oliver and Boyd, Edinburgh, p. 1–310.

TIFFNEY, B. H. 1977. Dicotyledonous angiosperm flower from the Upper Cretaceous of Martha's Vineyard. Massachusetts. Nature, 265:136–137.

TIFFNEY, B. H. 1984. Seed size, dispersal syndromes, and the rise of the angiosperms: evidence and hypothesis. Annals of the Missouri Botanical Garden, 71:551–576.

TITARENKO, S., P. J. WITHERS, AND A. YAGOLA. 2010. An analytical formula for ring artefact suppression in X-ray tomography. Applied Mathematics Letters, 23:1489–1495.

WEITKAMP, T., A. DIAZ, C. DAVID, F. PFEIFFER, M. STAMPANONI, P. CLOETENS, AND E. ZIEGLER. 2005. X-ray phase imaging with a grating interferometer. Optics Express, 13:6296–6304.

VIEHOFEN, A., C. HARTKOPF-FRÖDER, AND E. M. FRIIS. 2008. Inflorescences and flowers of *Mauldinia angustiloba* sp. nov. (Lauraceae) from mid-Cretaceous karst infillings in the Rhenish Massif, Germany. International Journal of Plant Sciences, 169:871–889.

VON BALTHAZAR, M., P. R. CRANE, K. R. PEDERSEN, AND E. M. FRIIS. 2011. New flowers of Laurales from the Early Cretaceous (early to middle Albian) of eastern North America, p. 49–87. *In* L. Wanntorp and L. P. Ronse De Craene (eds.), Flowers on the Tree of Life. Cambridge University Press, Cambridge.

VON BALTHAZAR, M., K. R. PEDERSEN, P. R. CRANE, AND E. M. FRIIS. 2008. *Carpestella lacunata* gen. et sp. nov., a new basal angiosperm flower from the Early Cretaceous (early to middle Albian) of eastern North America. International Journal of Plant Sciences, 169:890–898.

VON BALTHAZAR, M., K. R. PEDERSEN, P. R. CRANE, M. STAMPANONI, AND E. M. FRIIS. 2007. *Potomacanthus lobatus* gen. et sp. nov., a new flower of probable Lauraceae from the Early Cretaceous (early to middle Albian) of eastern North America. American Journal of Botany, 94:2041–2053.

ACCEPTED 8 OCTOBER 2013